NASA/TM—2014-216584

Viscoelastic Response of the Titanium Alloy Ti-6-4: Experimental Identification of Time- and Rate-Dependent Reversible and Irreversible Deformation Regions

Bradley A. Lerch and Steven M. Arnold
Glenn Research Center, Cleveland, Ohio

April 2014

NASA STI Program . . . in Profile

Since its founding, NASA has been dedicated to the advancement of aeronautics and space science. The NASA Scientific and Technical Information (STI) program plays a key part in helping NASA maintain this important role.

The NASA STI Program operates under the auspices of the Agency Chief Information Officer. It collects, organizes, provides for archiving, and disseminates NASA's STI. The NASA STI program provides access to the NASA Aeronautics and Space Database and its public interface, the NASA Technical Reports Server, thus providing one of the largest collections of aeronautical and space science STI in the world. Results are published in both non-NASA channels and by NASA in the NASA STI Report Series, which includes the following report types:

- TECHNICAL PUBLICATION. Reports of completed research or a major significant phase of research that present the results of NASA programs and include extensive data or theoretical analysis. Includes compilations of significant scientific and technical data and information deemed to be of continuing reference value. NASA counterpart of peer-reviewed formal professional papers but has less stringent limitations on manuscript length and extent of graphic presentations.

- TECHNICAL MEMORANDUM. Scientific and technical findings that are preliminary or of specialized interest, e.g., quick release reports, working papers, and bibliographies that contain minimal annotation. Does not contain extensive analysis.

- CONTRACTOR REPORT. Scientific and technical findings by NASA-sponsored contractors and grantees.

- CONFERENCE PUBLICATION. Collected papers from scientific and technical conferences, symposia, seminars, or other meetings sponsored or cosponsored by NASA.

- SPECIAL PUBLICATION. Scientific, technical, or historical information from NASA programs, projects, and missions, often concerned with subjects having substantial public interest.

- TECHNICAL TRANSLATION. English-language translations of foreign scientific and technical material pertinent to NASA's mission.

Specialized services also include creating custom thesauri, building customized databases, organizing and publishing research results.

For more information about the NASA STI program, see the following:

- Access the NASA STI program home page at *http://www.sti.nasa.gov*

- E-mail your question to *help@sti.nasa.gov*

- Fax your question to the NASA STI Information Desk at 443–757–5803

- Phone the NASA STI Information Desk at 443–757–5802

- Write to:
  STI Information Desk
  NASA Center for AeroSpace Information
  7115 Standard Drive
  Hanover, MD 21076–1320

NASA/TM—2014-216584

Viscoelastic Response of the Titanium Alloy Ti-6-4: Experimental Identification of Time- and Rate-Dependent Reversible and Irreversible Deformation Regions

Bradley A. Lerch and Steven M. Arnold
Glenn Research Center, Cleveland, Ohio

National Aeronautics and
Space Administration

Glenn Research Center
Cleveland, Ohio 44135

April 2014

Acknowledgments

This work was supported by NASA programs IVHM (Integrated Vehicle and Health Management) and SSAT (Systemwide Safety and Assurance Technologies). The authors appreciate the efforts of William Brown of Sierra Lobo, Inc., in preparing the test rig and samples. The texture measurements were performed by Dr. Richard Rogers of NASA. We also acknowledge the review comments of Dr. Tim Gabb, NASA Glenn.

Level of Review: This material has been technically reviewed by technical management.

Available from

NASA Center for Aerospace Information
7115 Standard Drive
Hanover, MD 21076–1320

National Technical Information Service
5301 Shawnee Road
Alexandria, VA 22312

Available electronically at http://www.sti.nasa.gov

Viscoelastic Response of the Titanium Alloy Ti-6-4: Experimental Identification of Time- and Rate-Dependent Reversible and Irreversible Deformation Regions

Bradley A. Lerch and Steven M. Arnold
National Aeronautics and Space Administration
Glenn Research Center
Cleveland, Ohio 44135

Summary

In support of an effort on damage prognosis, the viscoelastic behavior of Ti-6Al-4V (Ti-6-4) was investigated. This report documents the experimental characterization of this titanium alloy. Various uniaxial tests were conducted to low load levels over the temperature range of 20 to 538 °C to define tensile, creep, and relaxation behavior. A range of strain rates (6×10^{-07} to 0.001 s^{-1}) were used to document rate effects. All tests were designed to include an unloading portion, followed by a hold time at temperature to allow recovery to occur either at zero stress or strain. The titanium alloy was found to exhibit viscoelastic behavior below the "yield" point and over the entire range of temperatures (although at lower temperatures the magnitude is extremely small). These experimental data will be used for future characterization of a viscoelastic model.

Introduction

Under NASA's Systemwide Safety and Assurance Technologies (SSAT) project within the Aviation Safety Program the development, implementation, and experimental verification of a lifing (prognosis) methodology for structural components (e.g., jet engines) operating at high temperatures is underway. An objective of this program is to develop techniques to monitor vehicle condition and adjust performance profiles and maintenance schedules to ensure safe flight and long vehicle life. A key aspect of such a methodology is to correctly determine the extent of component degradation, thus requiring the deformation and damage behavior of the involved material to be well understood. In general, components are designed to operate in a material's elastic regime. However, there can be stressed locations in the component, loading and temperature anomalies, and other unusual events that cause permanent deformation to occur. With continued events the amount of deformation that the component experiences increases until local ductility is exhausted and a crack forms. Through a stress amplification process at the crack tip, the crack can then be easily driven through the component, causing a noticeable change in physical behavior, such as vibration, excess flexure, and acoustic events, to name a few, that should enable detection using a suitable diagnostic process. Given an accurate material model to assess the life of the component, the remaining structural capability of the component can be predicted and either repaired, removed from service, or have its service conditions changed.

A prerequisite for meaningful assessment of component durability and life, and consequently design of structural components, is the ability to accurately predict stresses, strains, failure modes, and their subsequent interaction and evolution occurring within a loaded structure. Furthermore, since constitutive material models provide the required link between stress and strain, this by necessity demands an appropriate constitutive behavior model for any material (be it monolithic or composite) before that material can be certified for use by a designer. Historically, metallic constitutive models have assumed the reversible or "elastic" regime to be time independent and the irreversible or "inelastic" strains to be either time independent ("plastic"), or at elevated temperatures, time dependent ("viscoplastic"). Prior research efforts on the titanium alloy TIMETAL 21S (Titanium Metals Corporation) determined that strains in the reversible regime can be both time independent and time dependent (Refs. 1 and 2)

depending on the temperature. Therefore concepts from viscoelasticity, which previously had not been typically applied to metals, actually need to be applied to the constitutive equations employed to analyze metals. Furthermore, in the regime of time-dependent strains, because of the wide spectrum of rate dependence of the material in both the reversible and irreversible domains, multiple mechanisms or relaxation spectra need to be included. The more mechanisms that are used, the more likely the characterized model is to appropriately predict the behavior across the range of service conditions. The GVIPS (generalized viscoplasticity with potential structure) model is a comprehensive viscoelastoplastic constitutive model that aims to describe a material's behavior whether in the viscoelastic or viscoplastic region (Refs. 3 and 4).

The GVIPS model was successfully characterized for the titanium alloy TIMETAL 21S in the above references. A logical extension to this would be to determine if this response is present in another, more widely used titanium alloy, Ti-6Al-4V (Ti-6-4). Ti-6-4 is an attractive candidate because it was estimated that 50 percent of all titanium used in aeroengine applications is Ti-6-4 (Ref. 5). For example, the alloy is commonly used for compressor blades and cases, fan blades and cases, fixtures, bolts, and tubing. The maximum use temperature of the material is generally assumed to be 427 °C (800 °F). However, to account for over-temperature excursions and local hot spots within components, testing is frequently performed at temperatures as high as 538 °C (1000 °F). Since this alloy was developed in the 1960s, one would assume there should be an extensive amount of data in the open literature available for model characterization. Unfortunately, although there have indeed been extensive studies performed on Ti-6-4, most (1) involve special cases (i.e., unusual heat treatments, varying microstructures, extreme load or temperature conditions, etc.), (2) provide limited data, or (3) provide inappropriate data for use in characterizing the model. Therefore, existing literature data did not help in restricting or reducing the amount of testing required for characterizing the GVIPS model and at best could only be used to provide limited guidance.

Consequently, the motivation behind the current study was to provide a sufficiently complete experimental database of response curves to enable the determination and full characterization of the viscoelastic response of the material (and the GVIPS constitutive model) over the service temperature range of interest to aeronautical engines. This report provides the experimental data itself, which will be used to characterize the viscoelastic model, the subject of a future report, and details on how these experiments were conducted. Future reports will address the viscoplastic and damage portions of the model. Data included in the current report are monotonic test results from low-level tensile, creep, and stress relaxation experiments. At the end of each test, the samples were unloaded and held for extended time at temperature and either at a fixed strain or stress level to permit full recovery of the deformation. Various loading rates were also employed. Finally, some of the basic viscoelastic parameters used in the model are calculated and discussed.

A list of symbols used in this report is given in Appendix A.

Experimental

For the given test program the Ti-6Al-4V material came from one lot of 16-mm-thick rolled plate, ordered to AMS specification 4911 (Ref. 6). The plate was received and used in the mill-annealed condition. The chemical composition was analyzed in house (Table I) and met the specification.

The supplier provided tensile properties at room temperature. These are listed in Table II and also satisfy the AMS 4911 specification.

Sections from the three primary directions of the plate were mounted, polished, and subsequently etched using Kroll's reagent to document the microstructure. Texture measurements were performed using an x-ray diffractometer equipped with a sealed Cu tube and a graphite monochrometer set to $K\alpha$ radiation. Pole figures were established for the plate.

TABLE I.—CHEMICAL COMPOSITION
OF Ti-6Al-4V PLATE

Element	Weight percent[a]
Al	6.28
V	3.85
Fe	0.15
O	0.14
C	0.035
N	0.01
Ti	Remainder
H	0.0070
Y	<0.005

[a]H and Y measurements were provided by material supplier.

TABLE II.—Ti-6Al-4V ROOM-TEMPERATURE TENSILE PROPERTIES[a]

Orientation	Yield strength, MPa (ksi)	Tensile strength, MPa (ksi)	Elongation, percent	Reduction in area, percent
Longitudinal	926 (134.3)	1003 (145.5)	15.0	42.6
Transverse	940 (136.3)	998 (144.7)	16.0	44.9

[a]Data were provided by material supplier.

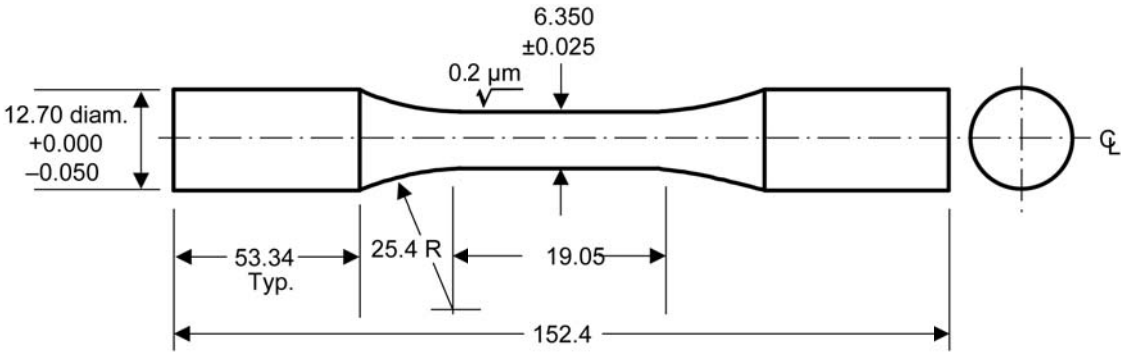

Figure 1.—Ti-6Al-4V test sample design (dimensions in millimeters).

Dynamic modulus tests were conducted on samples sectioned from the plate in the longitudinal (rolling) and short and long transverse (perpendicular to the rolling) directions. The samples were rectangular parallelepipeds, 40 by 12 by 3 mm in size. The tests were conducted using the impact vibration method from ASTM E1876 (Ref. 7). Tests were conducted from 28 to 700 °C in argon with data collected every 5 °C. The heating rate was 200 °C/h. The resulting resonance frequencies were on the order of 10 kHz. Both modulus of elasticity and shear modulus were measured; however, only modulus of elasticity is presented in this paper.

Static modulus was measured on every loaded sample. The modulus was measured at 20 °C using a manual cycle to stress levels of approximately ±14 MPa. Modulus measurements were occasionally taken at elevated temperature using a smaller load level. High-resolution stress and strain measurements were used for these tests. The modulus was also calculated from each viscoelastic test (be it tensile, creep, or relaxation) by fitting a line to the initial portion of the stress-strain curve.

Test samples were taken from the plate and machined to a 150-mm-long, cylindrical, dogbone sample having a 6.4-mm-diameter gauge section. The specimen design is given in Figure 1. The longitudinal axis of each sample was aligned parallel to the rolling direction of the plate. The samples had the final stock removed from the gauge using light passes to minimize residual stresses. The samples were not heat treated after machining. The gauge section had a final hand polish parallel to the longitudinal axis of the sample to ensure that the final machining marks were also parallel to the specimen's axis.

All specimens were tested on the same 50-kip (222-kN) hydraulically actuated load frame containing a 20-kip (89-kN) load cell. The 50-kip frame was used to provide good lateral stiffness. The specimens were held by water-cooled, hydraulically-actuated, collet-type grips. Axial alignment was checked using a strain-gaged sample and following the procedure used in ASTM E1012 (Ref. 8). The maximum bending strain at zero load was kept below 20 με.

Heating was accomplished using direct induction by means of a pair of three-wind copper induction coils. These coils provided a uniform temperature gradient along the sample gauge and maintained it to ±1 percent of the desired test temperature over the entire range of test temperatures. Temperature was measured using type-K thermocouples welded onto the sample. The temperature was measured and controlled at the bottom intersection between the specimen radius and the 12.7-mm grip end. This temperature was calibrated to a sample containing a total of five thermocouples welded both at this location and at four other points within the gauge length. This eliminated the welding of thermocouples onto actual samples (within the gauge length) and influencing the test results. It was discovered that the employed induction coil configuration not only provided an excellent thermal gradient, but it was very robust in that even larger-than-expected variations in thermocouple placement did not affect either the gradient or the absolute temperature. The test rig was enclosed by plastic shielding to minimize thermal drifts during the tests.

Axial strain was measured using a commercially available extensometer with Al_2O_3 probes for use at elevated temperatures. The gage length of the extensometer was 12.7 mm. The extensometer was water cooled for stability at high temperatures. The resolution of the extensometer at 538 °C was 2 με (1 με = 10^{-6} ε). Diametral strain was also measured on every sample using an optical micrometer. This allowed a diameter measurement to be taken at one point around the circumference of the sample and at a location just below the top radius of the sample. This device had a resolution at 538 °C of 0.002 mm, which equates to a strain of 300 με. The resolution of both extensometers improves as the temperature decreases.

Depending on the test type, tests were conducted in air either in load or strain control. The test procedure was

(1) Conduct a room-temperature modulus test in load control.
(2) Record the axial and diametral strain at zero load.
(3) Heat up the sample and hold for 15 to 30 min to achieve thermal equilibrium.
(4) Record the axial and diametral strain at zero load at the test temperature.
(5) Conduct a modulus test at the test temperature.
(6) Zero the axial extensometer, switch to strain control if warranted, and start the test.

Creep tests were conducted by loading in load control to the desired load value and holding for a period of 24 h. All tests were constant load (not stress) tests. Upon attaining the 24-h hold period, the load was removed and the specimen held at zero load for another 24 h and allowed to recover. The rate of loading was 0.001 s^{-1} (or its load equivalent $E\dot{e}$ where E is the static modulus at the test temperature and strain rate $\dot{e}$) unless otherwise indicated. The loading rate and unloading rate were always identical. Electronic noise increased with increasing temperature with the worst case being at 538 °C. The stress variation at 538 °C was approximately ±1 MPa during creep and ±0.35 MPa during recovery, indicating excellent control of the stress.

Stress relaxation tests were conducted in strain control to a predetermined strain level and held at that strain for 24 h to relax out the stress. After the 24-h period the specimen was unloaded to zero load, and the control mode was switched to load control. The sample was then held at zero load to recover (creep) for 24 h. Alternatively, a few tests were unloaded to zero strain and held for 24 h to recover through stress relaxation. The loading and unloading rates were again identical. The variation in strain due to noise was greatest at 538 °C and was approximately ±10 με.

Tensile tests were not conducted to failure for this report. Instead the loading portion of the creep and stress relaxation tests were used for tensile data. This also provided a larger number of replicates for assessing the specimen-to-specimen scatter. Alternate loading rates were occasionally employed, which ranged from 6×10^{-07} to 0.001 s^{-1} (or their equivalent elastic load rates). These rates represent the slowest rate that the test system could provide, and the fastest rate that the machine could accommodate without greatly overshooting the desired stress or strain limits. As will be shown later in this report, the fastest rate of 0.001 s^{-1} was sufficiently fast to lock in all time dependency of the material.

During the tests, computer acquisition of time, load, axial strain, and diametral strain was conducted. Data acquisition times varied from a point every 0.01 s to capture transient events, to every 120 s for capturing data over times of minimal changes (e.g., toward the end of a given creep or relaxation test). Additionally, signals were fed to both an x-y recorder and a strip chart recorder to verify data quality. The strip chart also had the advantage of capturing longer times (e.g., over the weekend) when the test had already terminated, but the load conditions were still being maintained, thus increasing the information over longer-than-planned test times. The x-y recorder provided an extra check on the modulus. At low loads, the analog recorder was able to filter out noise (which was contained in the digital signal) and often provided a better representation of the modulus.

Test Results

Microstructure

A three-dimensional view of the α-β microstructure is shown in Figure 2. The α grains (light phase) show elongation in all three directions, with the largest elongation noted along the rolling direction. The grain structure is inhomogeneous, making measurements of the average grain size unpractical. A rough estimate of the α-grain diameter is 6 μm, and the length in the rolling direction can be as much as 100 μm. Hardness was measured on the samples and was found to be HRC 30 and is consistent with the hardness of annealed Ti-6-4 in the literature (Refs. 9 and 10).

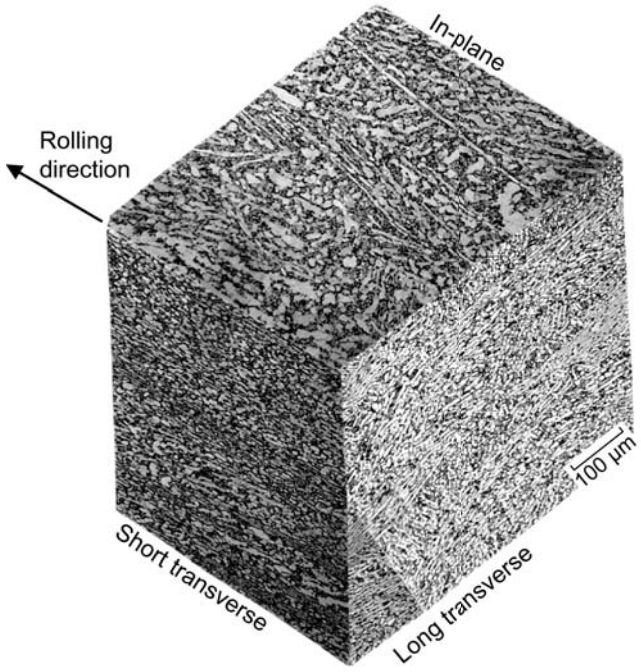

Figure 2.—Three-dimensional microstructure of 16-mm-thick Ti-6Al-4V plate.

Texture

Figure 3(a) shows the calculated full pole figures for the (0002) and $(10\bar{1}0)$ poles of the α Ti phase for the plate. The strong overlap of the β Ti (110) pole with both the α Ti (0002) and $(10\bar{1}1)$ poles prevented a successful extraction of β-phase pole figures. Values for selected maxima in the pole figures are indicated in units of multiples of a random distribution (m.r.d.). For a perfectly isotropic sample, m.r.d. = 1 at all points on a pole figure. The sample was found to have a transverse (T) texture, where the basal planes align perpendicular to the rolling plane with the c-axis parallel to the transverse direction (TD) as illustrated in Figure 3(b). Note from the $(10\bar{1}0)$ pole figure that the $(10\bar{1}0)$ pole (prismatic planes) tends to be parallel to the rolling direction (RD). To a lesser extent, this pole is also aligned with the thickness direction. A quantitative measure of texture sharpness is the texture index, which is computed from the orientation distribution function. Its value lies between 1 (for a texture-free sample) and infinity (for a single crystal). The texture index for this material was 1.55 indicating a moderate rolling texture.

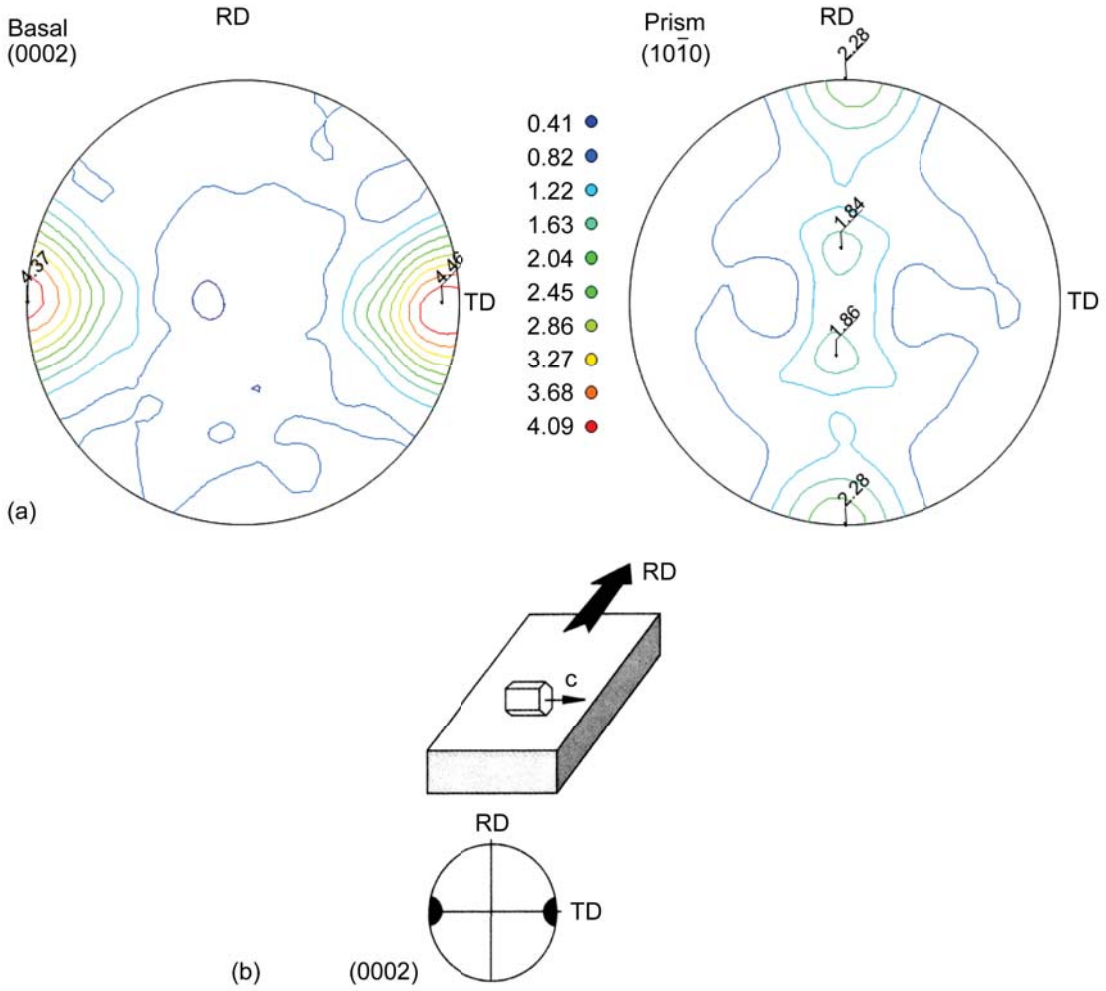

Figure 3.—Ti6Al-4V texture. (a) Pole figures for (0002) and $(10\bar{1}0)$ planes, where RD indicates rolling direction and TD, transverse direction. (b) Alignment of α-phase hexagonal close-packed crystal with respect to rolling direction of plate.

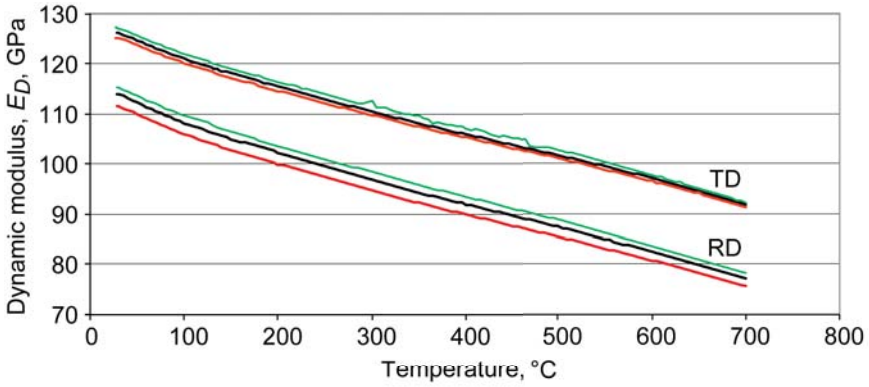

Figure 4.—Dynamic modulus E_D for Ti-6Al-4V samples in transverse (TD) and rolling (RD) directions as function of temperature.

Modulus

Dynamic modulus E_D measured in both transverse and longitudinal directions is shown in Figure 4. The solid lines represent the dynamic modulus for samples taken in all three planes both parallel (longitudinal) and perpendicular (transverse) to the rolling direction. Repeats were conducted for each orientation. Since the reproducibility is excellent, although it should be noted that the repeated samples were both taken out of the same area of the plate, only selected tests were plotted. The data show that the modulus in the transverse direction is noticeably higher than that in the longitudinal direction. At room temperature the modulus is 112 GPa for the longitudinal direction and 126 GPa for the transverse, representing a 12 percent difference in modulus. The dynamic modulus decreases linearly with increasing temperature until it is 77 and 91 GPa, for the longitudinal and transverse, respectively, at 700 °C, an approximate 30 percent drop over room temperature.

Viscoelastic Testing

Given that previous work on TIMETAL 21S showed the material to be viscoelastic and rate dependent (Ref. 2), it is assumed that Ti-6-4 will exhibit similar viscoelastic behavior at elevated temperatures. Consequently, it is important to establish the key viscoelastic parameters that define the viscoelastic model put forth in Saleeb and Arnold (Ref. 1) and Arnold, Saleeb, and Castelli (Ref. 2). The first is the identification of the threshold stress, κ, which represents the boundary between the reversible and irreversible domains. This can be determined exactly using the viscoelastic subtraction method put forth in Arnold, Saleeb, and Castelli (Ref. 2),

$$\kappa = \overline{\sigma} - E_S \varepsilon^{IR} \tag{1}$$

where $\overline{\sigma}$ is the applied stress level (just below the value of the proportional limit, *PL,* but above the threshold stress) where the creep test was held; E_S is the infinitely slow modulus, the stiffness that would be present if the material were loaded at an infinitely slow speed; and ε^{IR} is the irreversible strain determined after unloading and allowing sufficient time for all recovery to take place. Note that κ is the threshold stress in shear. For this work and since all of the tests conducted were uniaxial, future reference to κ will refer to the uniaxial stress value, *Y*. The two are related with the following relationship:

$$\kappa = \frac{Y}{\sqrt{3}} \tag{2}$$

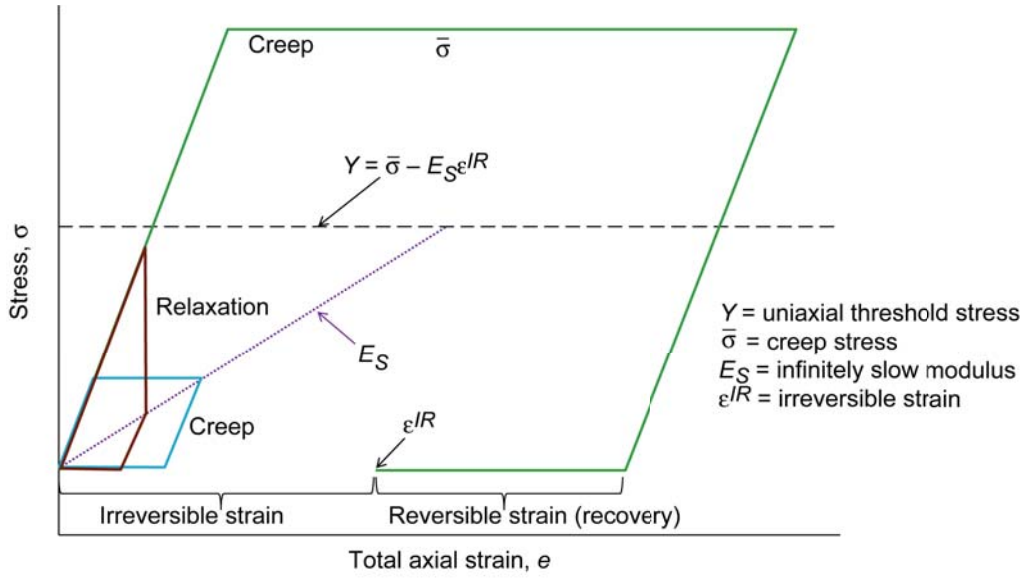

Figure 5.—Schematic depicting required testing for key viscoelastic parameters of Ti-6Al-4V.

Note the time-independent elastic modulus E_S needs to be found as does the full relaxation spectrum of the material; that is, for each of the viscoelastic mechanisms (i.e., Maxwell elements) introduced, the spring stiffness E_m and dashpot viscosities η (or relaxation time $\rho = E_m/\eta$) need to be computed. Furthermore, since the dynamic modulus of the material (E_D) is equal to the sum of the other stiffnesses,

$$E_D = E_S + \sum_{i=1}^{N} E_m^{(i)} \tag{3}$$

it is apparent that given E_D and E_S one can easily solve for the sum of the nonequilibrium stiffnesses. Figure 5 graphically depicts E_S and Y and indicates that they can be obtained at a given temperature by theoretically conducting as few as three tests: two creep or relaxation tests below the threshold stress Y (reversible) and a creep test above the threshold stress (irreversible). Consequently, brief descriptions of the tensile (T), creep (C), and relaxation (R) tests performed to obtain the necessary data follow. A list of all tests conducted for determining the viscoelasticity response of Ti-6-4 is given in Table III.

Tensile

Specimens were loaded in tension at a strain rate of 0.001 s^{-1} to a specified strain limit corresponding to a stress generally above the proportional limit (or apparent yield point) at a given temperature. For the purposes of this report, only the modulus and the yield points will be reported. A modulus at 20 °C was recorded before each test, and the average value was 116 GPa with a standard deviation of 2.8 GPa. The modulus and yield points are given in Table IV as a function of temperature, both decreasing as temperature increases. The modulus decreased 34 percent from 20 to 538 °C. The *PL* associated with a total strain rate of 0.001 s^{-1} decreased from 737 MPa at 20 °C to 114 MPa at 538 °C, a decrease of 85 percent. These values agree with those given in the Aerospace Structural Metals Handbook (Ref. 11) for annealed Ti-6-4.

TABLE III.—TEST MATRIX FOR VISCOELASTIC CHARACTERIZATION

Specimen[a]	Test type	Strain rate, s^{-1}	Loadup mode	Strain level[b]	Stress level,[b] MPa	Comments
(a) 20 °C						
17	Creep	0.001	Stress	0.0025	279	Below threshold stress *Y*
17C2	Creep	0.001	Stress	0.0050	558	
17C3	Creep	0.001	Stress	0.0056	629	
17C4	Creep	0.001	Stress	0.0063	698	
17R	Relaxation	0.001	Strain	0.0064	718	
17R2	Relaxation	0.001	Strain	0.0067	754	Above *Y*
17R3	Relaxation	0.001	Strain	0.0070	785	Above proportional limit *PL*
17R4	Relaxation	0.001	Strain	0.0073	814	
17R5	Relaxation	0.001	Strain	0.0076	844	
17C5	Creep	0.001	Stress	0.0083	891	
(b) 316 °C						
18	Creep	0.001	Stress	0.0028	275	Below *Y*
18R	Relaxation	0.001	Strain	0.0029	276	
18C	Creep	0.001	Stress	0.0045	441	
18C2	Creep	0.001	Stress	0.0045	441	
18C3	Creep	0.001	Stress	0.0049	479	Above *Y*
18C4	Creep	0.001	Stress	0.0059	547	
18T	Tensile	0.001	Strain	0.0180	650	
18TC	Creep	0.001	Stress	0.0087	274	
16R	Relaxation	0.001	Strain	0.0002	14	Below *Y*
16R2	Relaxation	0.001	Strain	0.0004	38	
16R3	Relaxation	0.001	Strain	0.0007	72	
16C	Creep	0.001	Stress	0.0010	103	
16R4	Relaxation	0.001	Strain	0.0014	141	
16R5	Relaxation	0.001	Strain	0.0021	197	
16C2	Creep	0.001	Stress	0.0024	236	
16C3	Creep	0.001	Stress	0.0027	270	
16C4	Creep	0.001	Stress	0.0031	304	
16R6	Relaxation	0.001	Strain	0.0034	344	
16R7	Relaxation	0.001	Strain	0.0167	636	Above *Y*
54C	Creep	0.001	Stress	0.0025	237	Below *Y*
54C2	Creep	0.001	Stress	0.0032	309	
54C3	Creep	0.001	Stress	0.0039	377	
54C4	Creep	0.001	Stress	0.0045	447	
54C5	Creep	0.001	Stress	0.0049	482	
54C6	Creep	0.001	Stress	0.0053	515	
54C7	Creep	0.001	Stress	0.0057	549	Above *Y*
54C8	Creep	0.001	Stress	0.0063	596	
54R	Relaxation	0.001	Strain	0.0180	650	
(c) 371 °C						
59R	Relaxation	0.001	Strain	0.0014	132	Below *Y*
59C	Creep	0.001	Stress	0.0015	138	Below *Y*
59C2	Creep	0.001	Stress	0.0037	344	Above *Y*
59R2	Relaxation	0.001	Strain	0.0180	599	Unload to zero strain (2 cycles)

TABLE III.—Concluded.

(d) 427 °C

25C	Creep	0.001	Stress	0.0004	34	Below *Y*
25R	Relaxation	0.001	Strain	0.0004	39	
25R2	Relaxation	0.001	Strain	0.0008	74	
25C2	Creep	0.001	Stress	0.0023	206	Above *Y*
25R3	Relaxation	0.001	Strain	0.0180	585	Above *Y*
26R1	Relaxation	0.001	Strain	0.0004	34	
26R2	Relaxation	0.0000008	Strain	0.0004	34	Below *Y*, below slow-rate *PL*
26R3	Relaxation	0.001	Strain	0.0004	35	Repeat of R1
26C1	Creep	0.0000008	Stress	0.0008	68	Below *Y*, above slow-rate *PL*
26C2	Creep	0.001	Stress	0.0026	239	Above *Y*, below fast-rate *PL*
26C3	Creep	0.0024	Stress	0.0048	445	Above *Y*, below fast-rate *PL*
8R	Relaxation	0.001	Strain	0.0011	103	Below *Y*
7C1	Creep	0.001	Stress	0.0040	36	Had prior test at 552 MPa
7C2	Creep	0.001	Stress	0.0006	55	Below *Y*
7C3	Creep	0.001	Stress	0.0009	82	
7C4	Creep	0.001	Stress	0.0011	96	
7C5	Creep	0.001	Stress	0.0014	123	
7C6	Creep	0.001	Stress	0.0017	151	
7C7	Creep	0.001	Stress	0.0020	178	
7C8	Creep	0.001	Stress	0.0028	247	Above *Y*
7C9	Creep	0.001	Stress	0.0035	316	Above *Y*
83C	Creep	0.001	Stress	0.0008	70	Below *Y*
83C1	Creep	0.001	Stress	0.0010	97	Below *Y*
83C2	Creep	0.001	Stress	0.0026	243	Above *Y*
83C4	Creep	0.001	Stress	0.0122	577	Above *Y*
83C5	Creep	0.001	Stress	0.0008	70	Below *Y*
83C6	Creep	0.001	Stress	0.0011	97	Below *Y*
83C7	Creep	0.001	Stress	0.0027	243	Above *Y*

(e) 482 °C

47R	Relaxation	0.001	Strain	0.0002	15	Below *Y*
47C	Creep	0.001	Stress	0.0001	14	Below *Y*
47C2	Creep	0.001	Stress	0.0008	69	Above *Y*
47R2	Relaxation	0.001	Strain	0.0179	553	Unload to zero strain (2 cycles)

(f) 538 °C

28	Creep	0.001	Stress	0.0001	7	Below *Y*
28R	Relaxation	0.001	Strain	0.0002	16	Below *Y*
28C	Creep	0.001	Stress	0.0004	33	Above *Y*
28C2	Creep	0.001	Stress	0.0004	33	
28T	Tensile	0.001	Strain	0.0038	294	
28T2	Tensile	0.001	Strain	0.0178	502	
28TR	Relaxation	0.001	Strain	0.0002	14	Below *Y*
28TC	Creep	0.001	Stress	0.0002	14	Below *Y*
28TC5	Creep	0.001	Stress	0.0004	33	Above *Y*
92R	Relaxation	0.001	Strain	0.0001	8	Below *Y*
92C	Creep	0.001	Stress	0.0001	7	Below *Y*
92C2	Creep	0.001	Stress	0.0004	34	Above *Y*
92R2	Relaxation	0.001	Strain	0.0179	508	Unload to zero strain
60R	Relaxation	0.001	Strain	0.0001	7	Below *Y*
60C1	Creep	0.00000063	Stress	0.0020	104	Above *Y*

[a]Test specimens are designated by sample number, test type (C is creep; R, relaxation; and T, tensile), and test number.
[b]Values for response signal taken at the end of the loadup.

TABLE IV.—TENSILE PROPERTIES AND KEY VISCOELASTIC PARAMETERS FOR VISCOELASTIC TESTS

Test temperature, °C	Sample number	Tensile properties[a]				Viscoelastic parameters		
		Elastic modulus, *E*, GPa	Proportional limit, *PL*, MPa	0.02% yield point, MPa	0.2% yield point, MPa	Infinitely slow modulus, E_S, GPa	Threshold stress, *Y*, MPa	*Y*/*PL*
538	28	84.19	105	261	397	21.3	16.5	0.16
538	92	86.39	122	215	471	30.5	15.6	0.13
538	60	82.46	20	59	---	6.6	---	---
482	47	84.81	303	431	513	52.6	37.8	0.12
482	14	87.29	178	354	484	---	---	0.22
427	25	89.98	476	506	533	68.8	170.9	0.36
427	83	93.15	473	518	552	73.9	217.1	0.46
427	63	90.53	---	---	---	65.5	90.5	---
427	26	91.70	---	---	---	75.4	199.7	---
427	8	91.63	---	---	---	55.6	---	---
371	59	94.19	502	529	553	80.6	316.3	0.63
316	18	97.50	593	616	600	95.7	461.9	0.78
316	16	98.46	525	547	575	97.0	>344.8[c]	0.66
316	54	96.19	603	651	632	95.5	517.8	0.86
200	50	103.36	587	640	677	102.3	516.6	0.88
100[b]	---	---	---	---	---	107.3	634.3	0.91
20	10	112.60	846	883	926	112.6	795.4	0.94
20	17	111.70	737	880	---	110.8	732.8	0.99

[a]At strain rate of 0.001 s^{-1}.
[b]Values at this temperature were interpolated.
[c]This was the highest value measured that was still reversible. The next test in this series was taken at the 0.2% yield point.

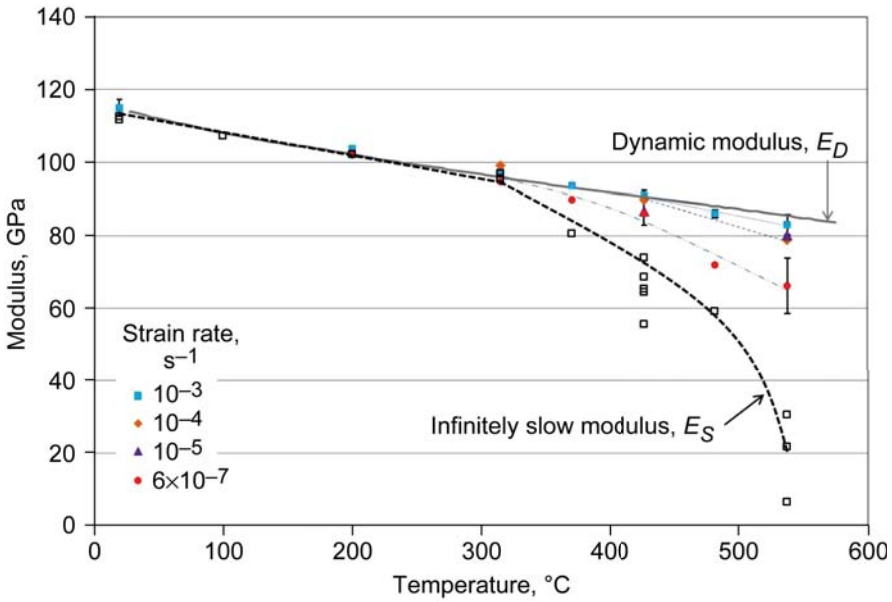

Figure 6.—Modulus for Ti-6Al-4V as function of temperature and strain rate.

Modulus is plotted in Figure 6 as a function of temperature and strain rate. The solid line is the dynamic modulus data taken from Figure 4 for the longitudinal direction. The solid points in Figure 6 represent the static modulus calculated from individual test samples in the overall program and cover the entire range of strain rates. In general, the modulus is shown to decrease with increasing temperature, for both the dynamic and static tests. At low temperatures, the modulus for the cylindrical samples (static modulus) coincides with the data for the dynamic tests and this is to be expected since (1) the modulus

was measured in the same direction (along the rolling direction) and (2) at low temperatures rate dependence is not anticipated. However, at approximately 316 °C, strain rate becomes important, and the static modulus deviates from those of the dynamic data. This drop becomes more drastic as the applied strain rate decreases. Dotted lines are drawn in to aid in the discrimination of the various strain rates. Error bars representing one standard deviation on the static modulus are shown where there is sufficient data. At 538 °C the modulus for the slowest strain rate (6×10^{-07} s^{-1}) is only 63 GPa, which is 20 GPa lower than the dynamic modulus at the same temperature. Note, however, that for strain rates equal to or faster than 1×10^{-05} s^{-1}, the modulus is still approximately the same as the dynamic tests, which has a strain rate on the order of 1.0 s^{-1}. Hence there is a strain rate effect on modulus starting at approximately 316 °C, with a slower strain rate leading to a lower modulus. The rate effect increases with increasing temperature as one would expect. The remaining curve (dashed line) is the calculated stiffness E_S representing the modulus at an infinitely slow strain rate (to be explained later).

The *PL* values, threshold, and 0.02 and 0.2 percent yield points are shown in Figure 7 as a function of temperature. These values were taken from individual tests loaded at a strain rate of 0.001 s^{-1}. Error bars for ±1 standard deviation are again given where sufficient data were available. Smooth curves were drawn through all points associated with the same yield definition to facilitate the observation of a decreasing yield with increasing temperature. The final set of data represents the threshold values calculated from Equation (1). It is noteworthy that the threshold values fall significantly below those of the fast-rate proportional limit.

Creep

Several creep tests were performed at various temperatures below the corresponding apparent yield points. Specimens were loaded at a rapid load rate (the elastic equivalent of a strain rate of 0.001 s^{-1}) in an attempt to lock in all time dependency. Initial levels for a given specimen were maintained in the reversible regime (below *Y*) whereas final stress levels for a given specimen were in the irreversible regime (above *Y*). Representative response curves from a given specimen are shown in Figure 8, where both creep and recovery (where the time at which the load was removed was reset to zero) portions of the curves are shown for loads below *Y* (14 MPa) and above *Y* (69 MPa). The salient features for samples loaded in the reversible regime are that at a constant load, an initial primary creep region is observed followed by a shutdown of creep, thereafter yielding a constant strain with respect to time.

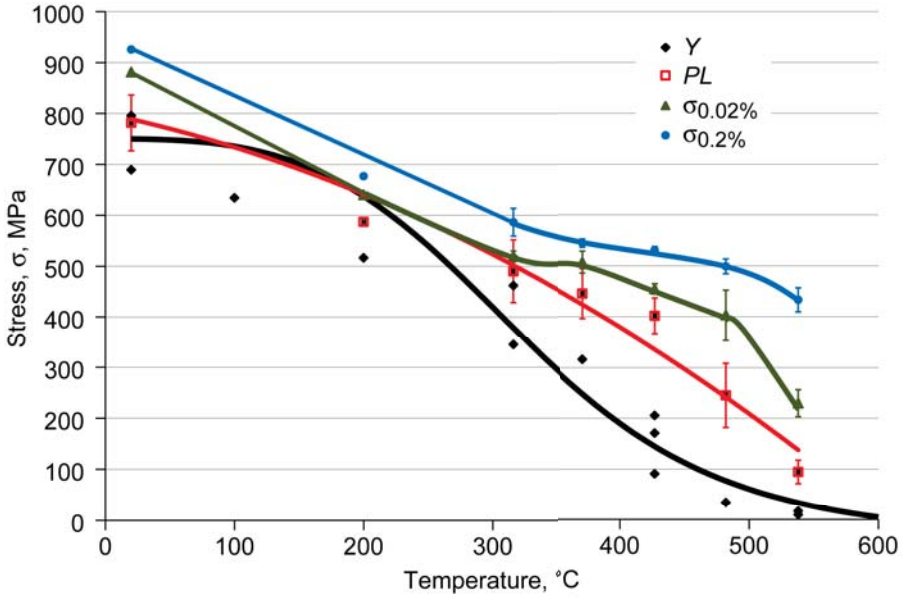

Figure 7.—Ti-6Al-4V temperature dependence of 0.02% and 0.2% yield points $\sigma_{0.02\%}$ and $\sigma_{0.2\%}$ (strain rate = 1×10^{-3} s^{-1}), threshold stress *Y*, and proportional limit *PL*.

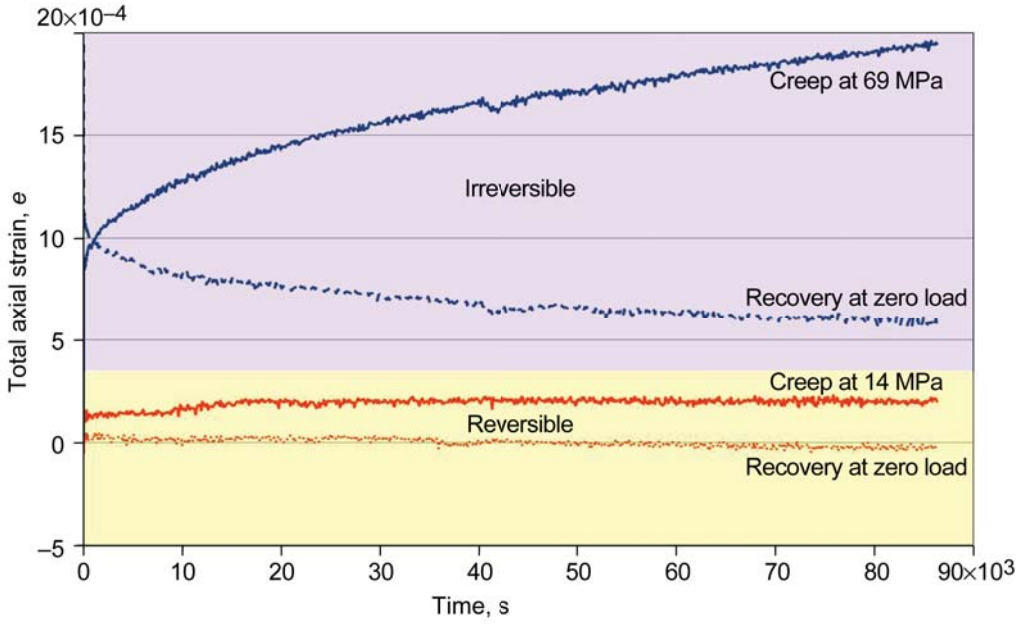

Figure 8.—Creep and recovery curves for Ti-6Al-4V in the reversible and irreversible regimes.

Consequently, no secondary creep regime is experienced, which is consistent with full strain reversibility.[1] The reversibility is confirmed by unloading to zero load, and holding this load at temperature for 24 h. This is in contrast to behavior in the irreversible regime, during which primary creep transitions to nonzero secondary creep (see the solid blue line). Upon unloading the specimen experiences some recovery but does not return to zero strain as it did in the reversible regime, and maintains a permanent strain offset (e.g., in Fig. 8 the 69 MPa load case recovers to approximately 600 με).

Relaxation

Relaxation tests were also performed in both the reversible and irreversible regimes. Tests were conducted with a loading-unloading total strain rate of 0.001 s^{-1}, again to lock in all time dependency. A representative response curve for a sample tested in the reversible regime at 371 °C and held at a total strain of 0.0014 is shown in Figure 9. The stress in the sample relaxed 22 percent during the 24-h hold with saturation (relaxation shutdown) σ_{sat} near the end of the hold period. Similar behavior is also observed at 427 °C for relaxation at 0.0011 total strain, wherein the stress in the sample relaxed 38 percent. Upon unloading to zero stress and switching to stress control, the strain recovered to zero. A relaxation test at 427 °C that was unloaded to zero strain and then recovered is shown in Figure 9 (see the dashed line). Note that at zero strain (the time at which this occurred has been reset to zero in the figure) the specimen had a compressive stress of 40 MPa, which almost completely recovered to near zero after 40 h. Relaxation in the irreversible regime neither shuts down, nor does the specimen recover to zero upon unloading.

[1]A secondary creep rate of zero is a definite indication of reversibility only at elevated temperatures where a thermal recovery exists. At low temperatures, thermal recovery is very small and a zero creep rate does not necessarily imply reversibility. To document reversibility in this case the sample has to be unloaded and fully recover.

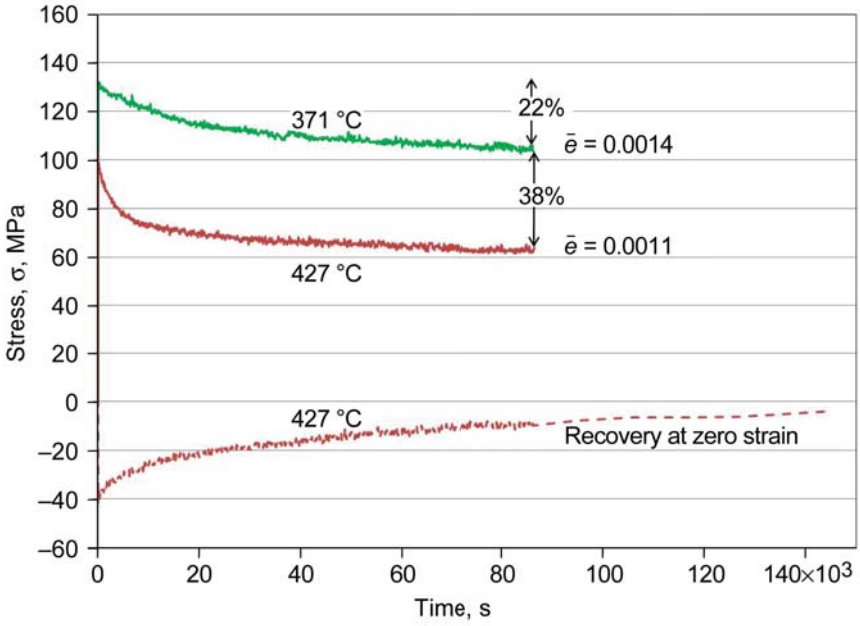

Figure 9.—Relaxation and recovery (strain rate = 1×10^{-3} s^{-1}) for Ti-6Al-4V in reversible regime at two temperatures, where $\bar{e}$ is relaxation strain.

Both creep (C) and relaxation (R) data at each test temperature (often for multiple specimens) are given in Figures 10 to 21. For each temperature a plot of stress-strain and strain-time is shown for both loading and recovery portions of the test. In these plots, the response variables advance continuously, and time is not reset to zero upon unloading. Also shown in these plots is the delineation between reversible and irreversible deformation as indicated by Y. For stress versus time and/or strain plots, Y is a straightforward limit value and is shown by a box representing the range of values for the various samples. However, in strain-time space one needs to develop a corresponding range. Consequently, the upper reversible strain bound (i.e., the accumulated strain after "infinite" amount of time) is represented by $\varepsilon^{R}_{\max} = Y/E_S$, where the minimum and maximum values for E_S were used to calculate this upper strain limit. The values of E_S used either represent the within-sample scatter when there is only one sample per temperature or the within-temperature values for multiple specimens. Similarly, the maximum achievable, instantaneous reversible (i.e., elastic) loadup strain is determined using the expression Y/E_D. Comparing this value with the strain value after loadup of a given test, one can immediately observe if the test is above or below the threshold. In Figure 11 both E_D and E_S were used to calculate these ranges. Consequently, the instantaneous strain equivalent for Y (using E_D) is the best indicator of the boundary between reversible and irreversible deformation in the strain-time space. This maximum elastic strain (Y/E_D) is shown in Figure 11, whereas on almost all other strain-time plots only the upper reversible strain limit Y/E_S is shown. For both these calculations a range is usually given rather than a single value. This is because the values of E_D and E_S are typically from multiple samples. If only one sample was tested per temperature, within-sample values of E_S were used to calculate the range. It should also be noted that all of the stress-strain curves from Figures 10 to 21 show linear behavior during loading of the sample.

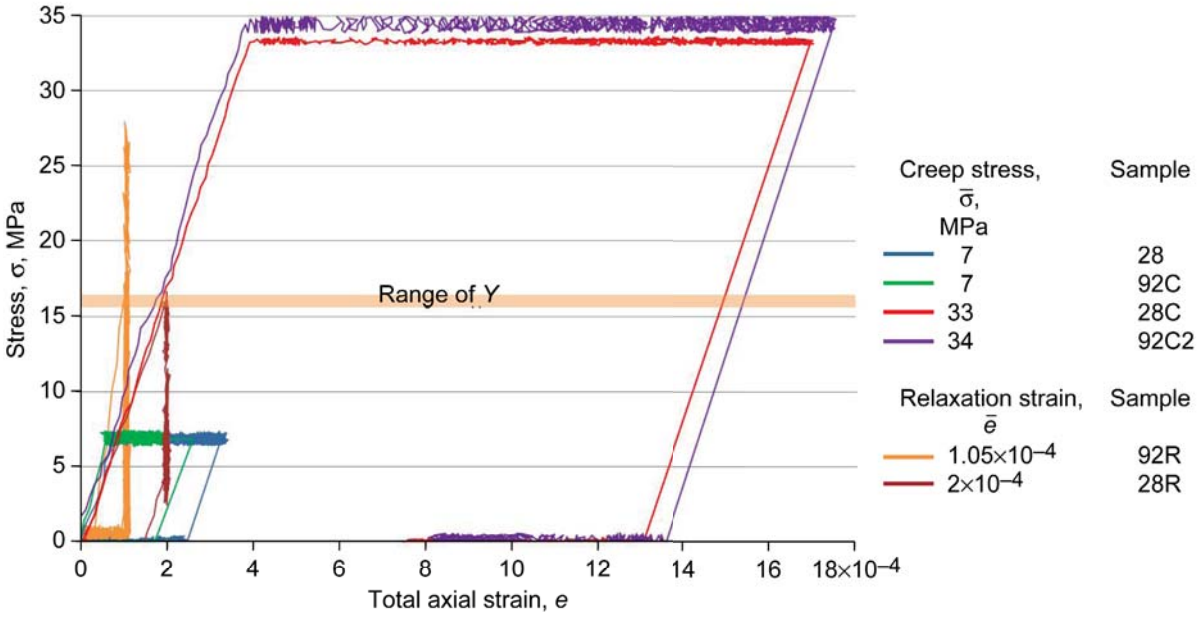

Figure 10.—Stress-strain response of Ti-6Al-4V for viscoelastic tests at 538 °C, showing range of threshold stress *Y*.

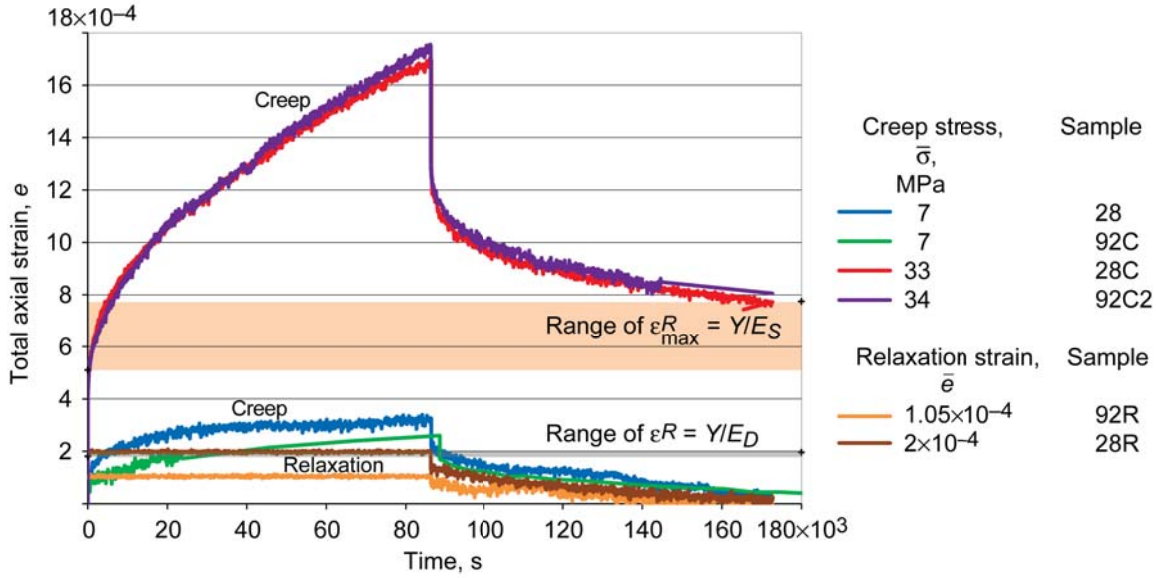

Figure 11.—Strain-time response of Ti-6Al-4V for viscoelastic tests at 538 °C, where ε^R_{max} is maximum reversible strain, εR is reversible strain, Y is threshold stress, E_S is infinitely slow modulus, and E_D is dynamic modulus.

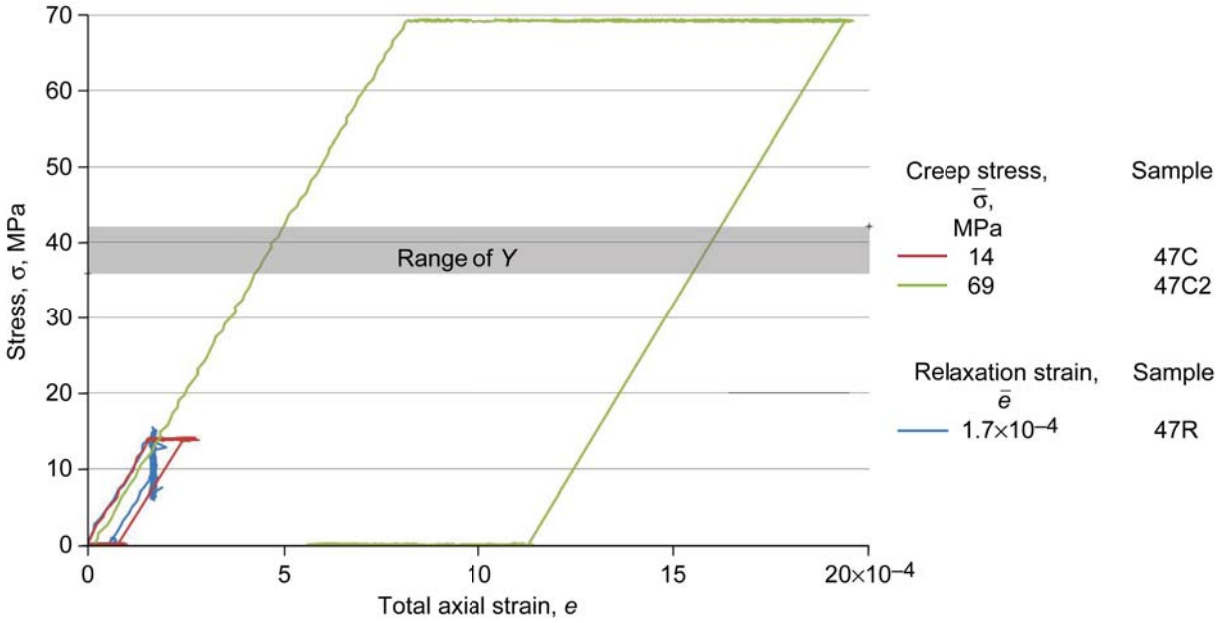

Figure 12.—Stress-strain response of Ti-6Al-4V for viscoelastic tests at 482 °C, showing range of threshold stress *Y*.

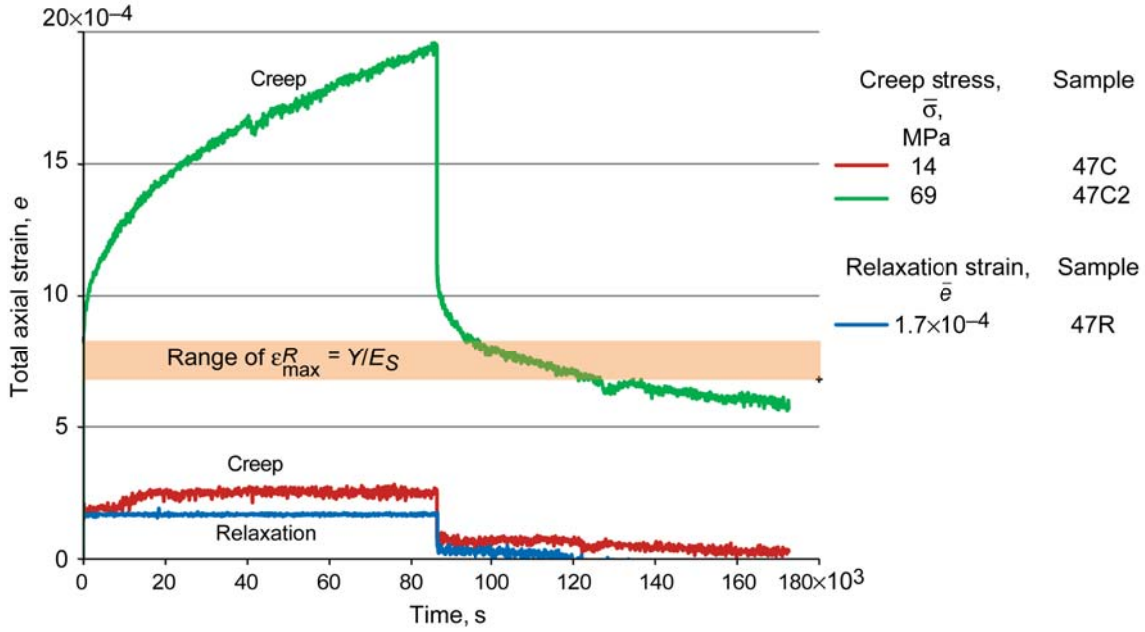

Figure 13.—Strain-time response of Ti-6Al-4V for viscoelastic tests at 482 °C, where ε^R_{max} is maximum reversible strain, *Y* is threshold stress, and E_S is infinitely slow modulus.

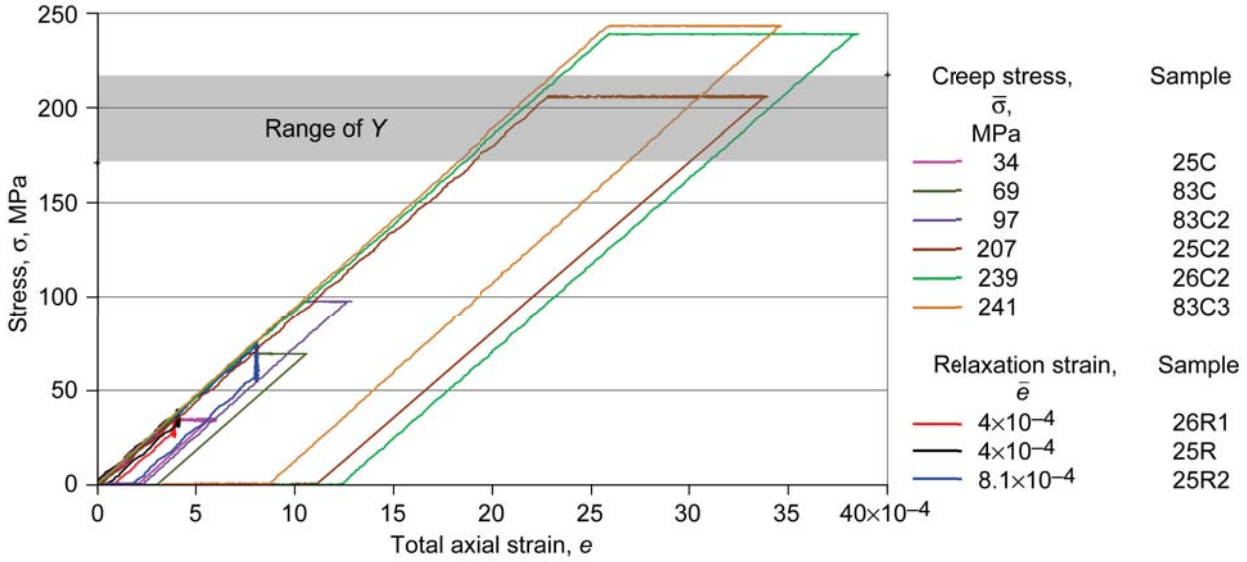

Figure 14.—Stress-strain response of Ti-6Al-4V for viscoelastic tests at 427 °C, showing range of threshold stress *Y*.

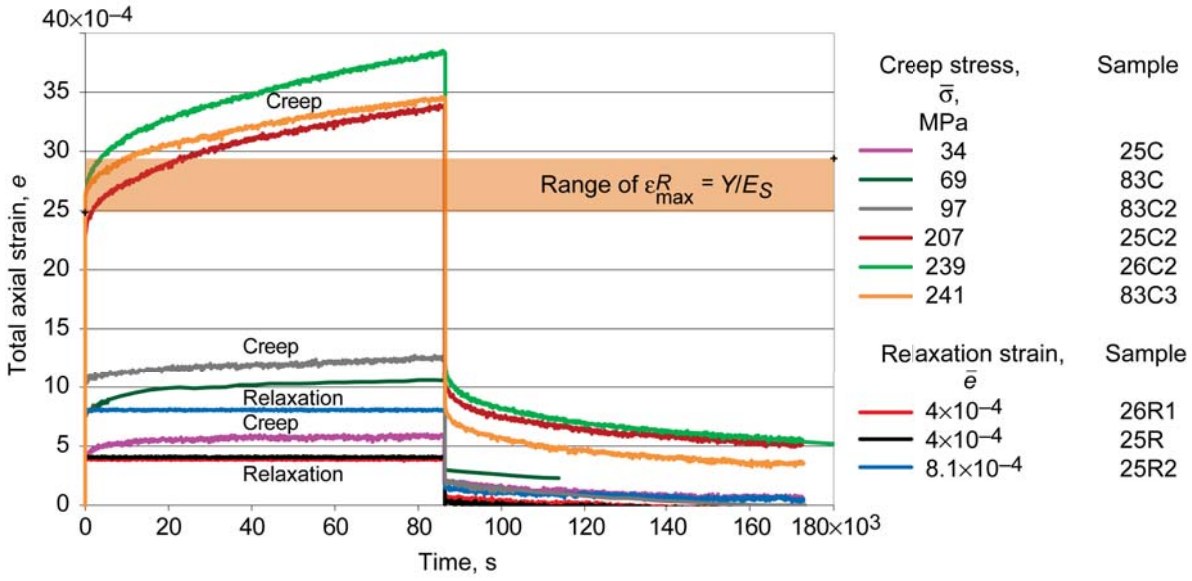

Figure 15.—Strain-time response of Ti-6Al-4V for viscoelastic tests at 427 °C, where ε^R_{max} is maximum reversible strain, *Y* is threshold stress, and E_S is infinitely slow modulus.

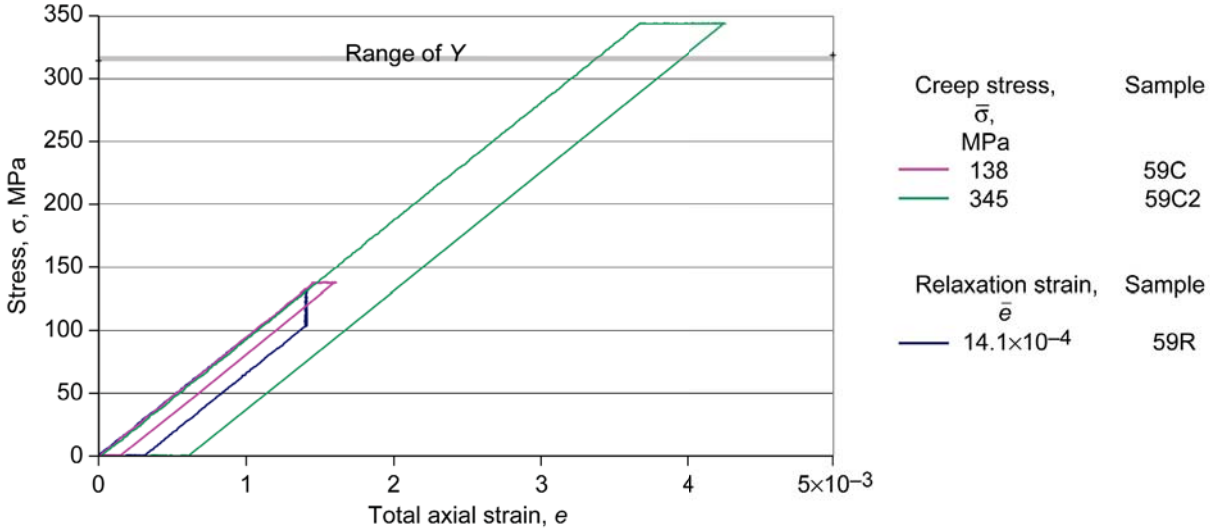

Figure 16.—Stress-strain response of Ti-6Al-4V for viscoelastic tests at 371 °C, showing range of threshold stress *Y*.

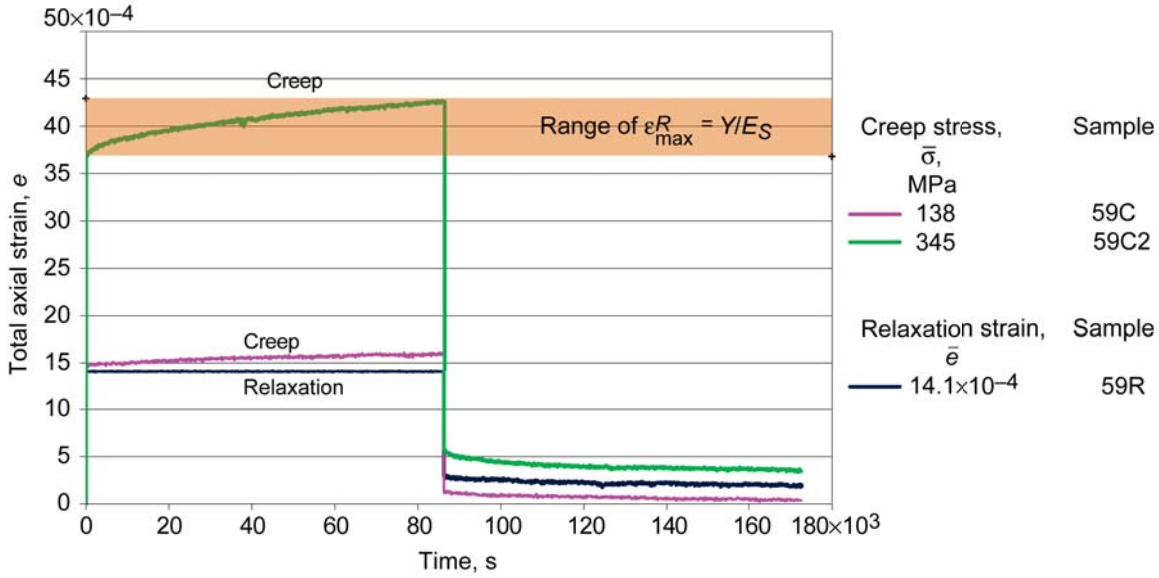

Figure 17.—Strain-time response of Ti-6Al-4V for viscoelastic tests at 371 °C, where ε^R_{max} is maximum reversible strain, *Y* is threshold stress, and E_S is infinitely slow modulus.

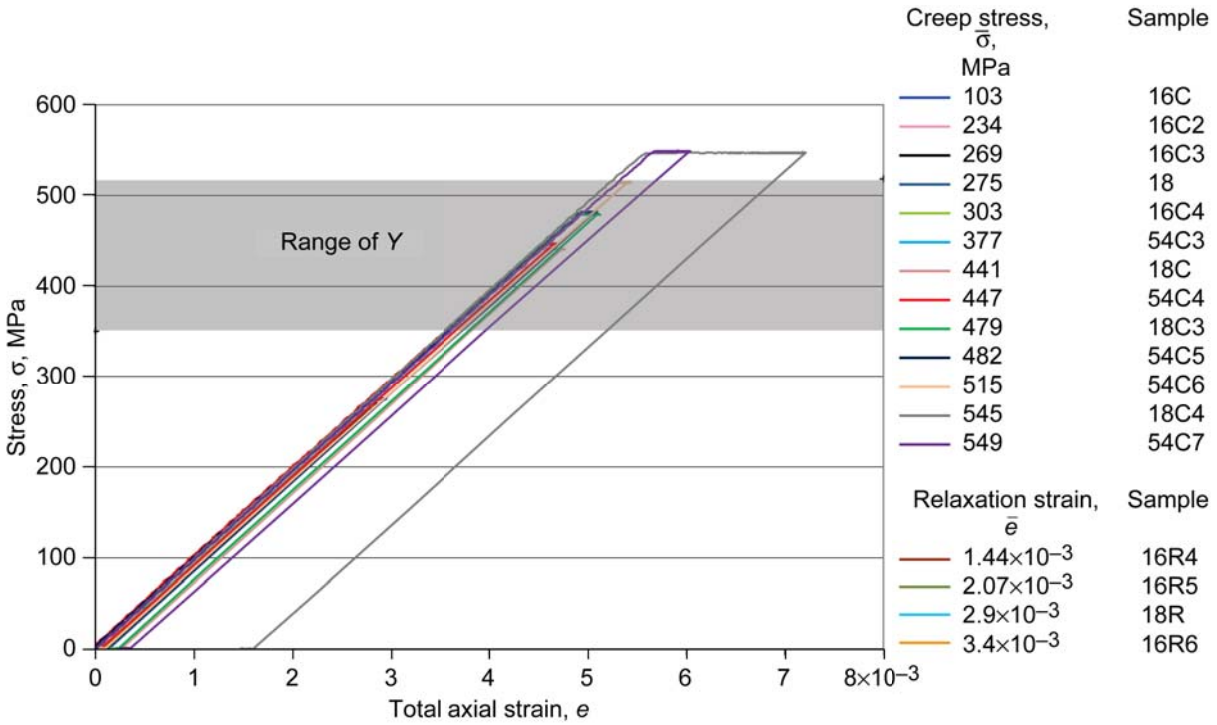

Figure 18.—Stress-strain response of Ti-6Al-4V for viscoelastic tests at 316 °C, showing range of threshold stress *Y*.

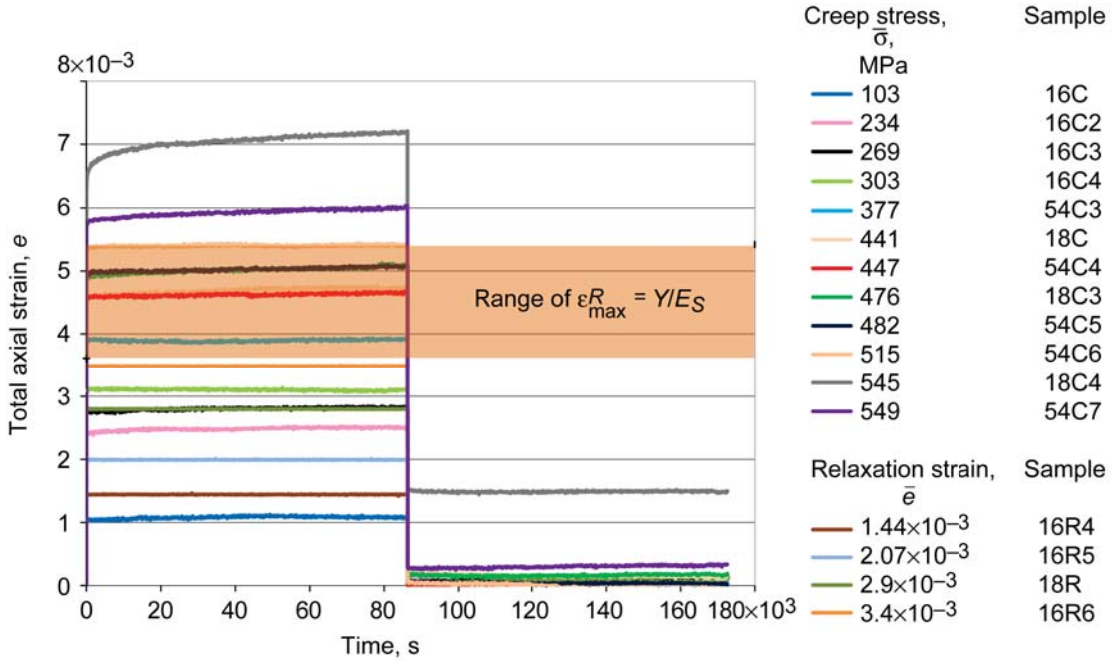

Figure 19.—Strain-time response of Ti-6Al-4V for viscoelastic tests at 316 °C, where ε^R_{max} is maximum reversible strain, *Y* is threshold stress, and E_S is infinitely slow modulus.

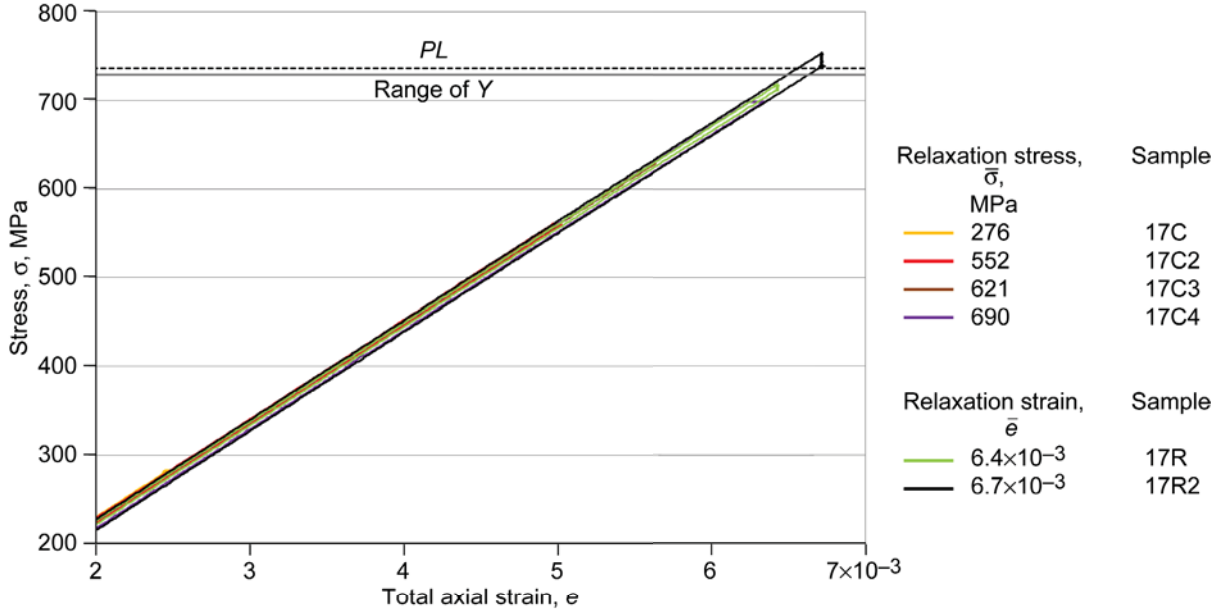

Figure 20.—Stress-strain response of Ti-6Al-4V for viscoelastic tests at 20 °C, showing proportional limit *PL* and range of threshold stress *Y*.

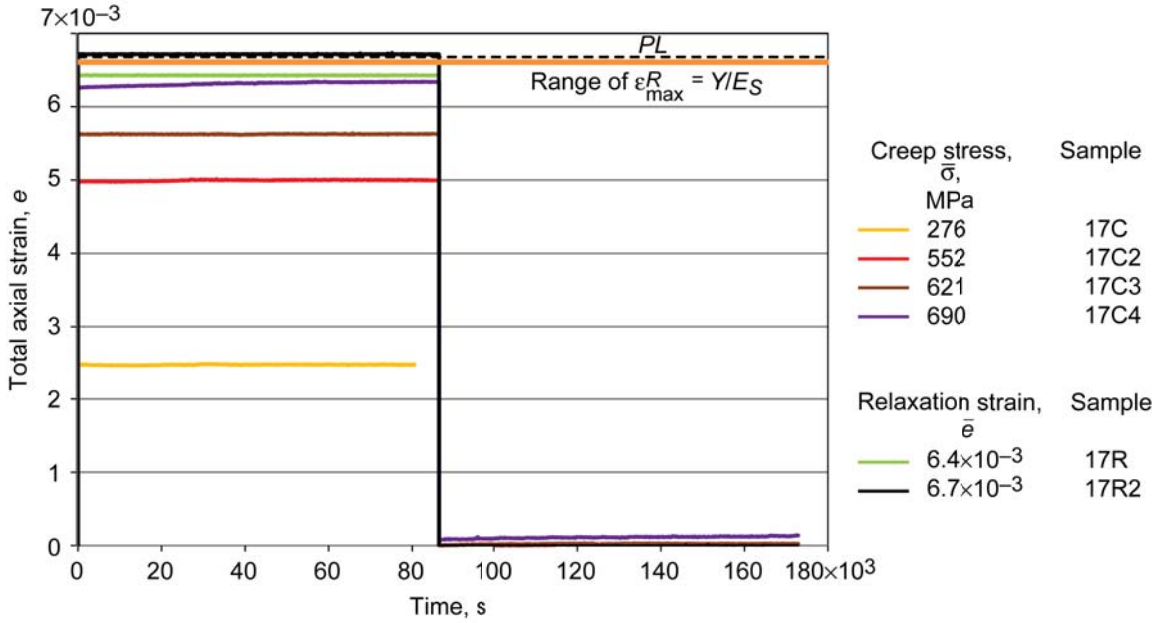

Figure 21.—Strain-time response of Ti-6Al-4V for viscoelastic tests at 20 °C, where *PL* is proportional limit, ε^R_{max} is maximum reversible strain, *Y* is threshold stress, and E_S is infinitely slow modulus.

Room-Temperature Testing

A viscoelastic test series was conducted on sample 17 at 20 °C to examine if viscoelasticity is active at such low temperatures. Time-dependent deformation both under creep and relaxation have been observed in Ti-6-4 at room temperature (Refs. 9 and 12 to 18) and other titanium alloys (Refs. 15 and 19 to 21). Here the objective will be to determine if this behavior is limited to the irreversible regime alone. The test series is shown in Figures 20 and 21. Four creep tests were conducted at low loads, followed by five relaxation tests that are situated both below and above the proportional limit, and finally ending with a high-stress creep test. Figure 20 shows that *PL* is high at 20 °C, and the corresponding amount of time-dependent behavior is exceedingly small. This is also shown in Figures 21 and 22 where an identifiable amount (<100 με) of creep can be observed starting at a stress of 690 MPa. A better view of the time dependence can be seen by removing the loading strains and plotting only creep strain (i.e., strain accumulation subsequent to loadup) as in Figure 22. Here, time dependency can be observed at stresses as small as 552 MPa. At a still higher stress of 690 MPa (test 17C4) almost 100 με of creep (approximately 1.6 percent of the total strain) can be seen with an apparent shutdown at about 60 000 s. Upon unloading, the tests recover to near zero strain (Fig. 23) up through 690 MPa.

The next five tests were relaxation tests and their stress responses are shown in Figure 24. Only the test at the lowest strain (0.0064) lies below *Y*. Relaxation at stresses near *Y* shows a stress drop of 6 MPa (1 percent) for a strain level of 0.0064 (below *Y*) and a stress drop of 14 MPa (2 percent) for a strain level of 0.0067 (above *Y*), indicating measurable time dependency. These tests were subsequently unloaded to zero strain and held to recover through stress relaxation as shown in Figure 25 (with the time reset to zero). Although none of the samples relaxed back to zero stress, the two tests at the lowest strain levels could be considered to have fully reversed within experimental error. Calculation of two of the viscoelastic parameters for this sample yielded E_S = 110.8 GPa and Y = 732.8 MPa. The fast-rate modulus for this sample was 111.7 GPa and indicates that $E_S < E_D$ by 0.9 GPa. Likewise $Y < PL$ by 4.2 MPa. Hence, viscoelasticity provides a very small part (<2 percent) of the reversible deformation at room temperature, with 98 percent being time-independent elastic response.

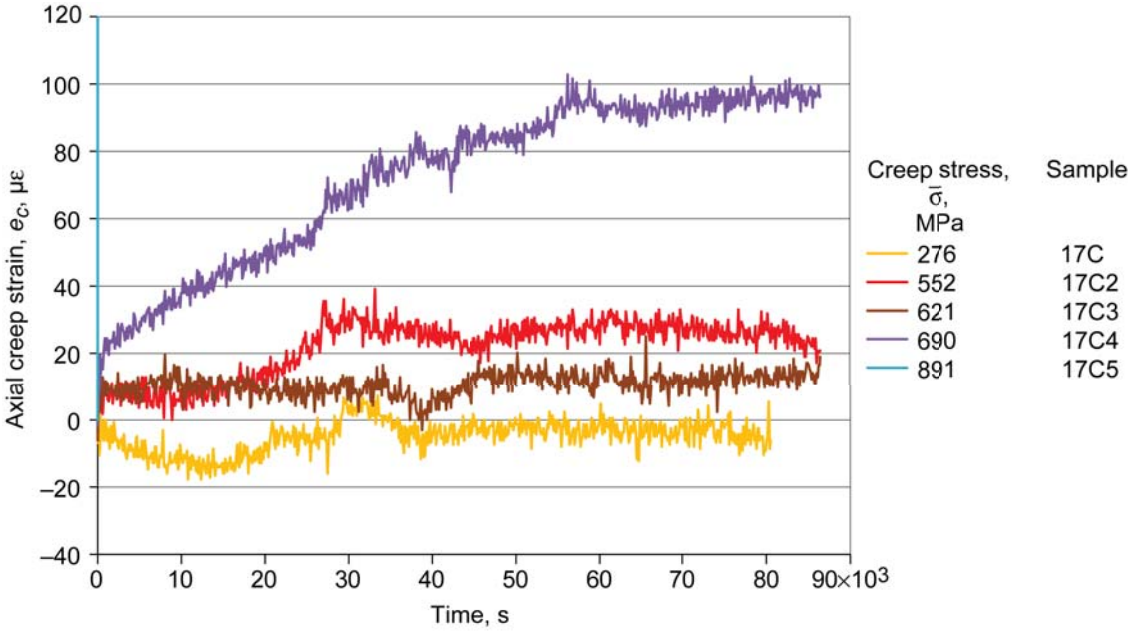

Figure 22.—Axial creep strain for Ti-6Al-4V at various stress levels at 20 °C.

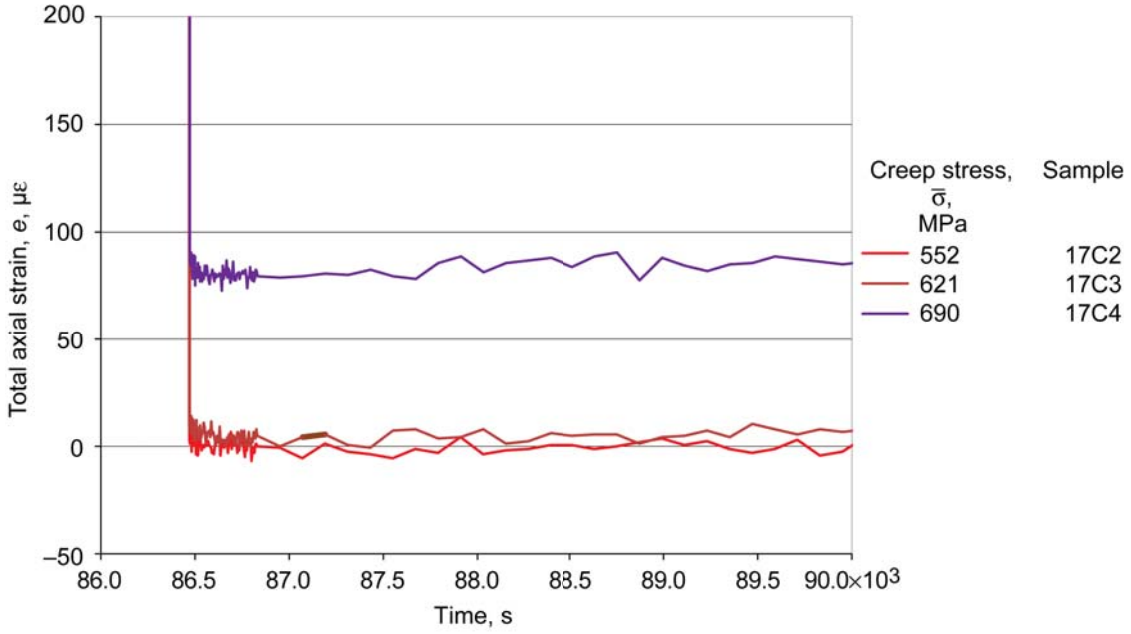

Figure 23.—Axial strain recovery for Ti-6Al-4V at various stress levels at 20 °C.

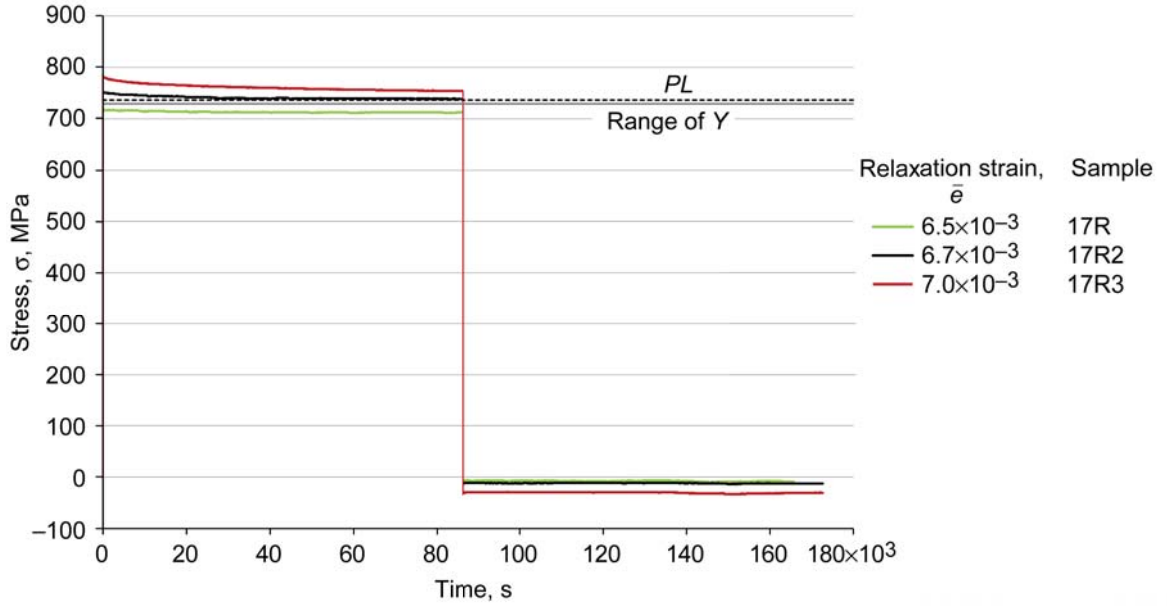

Figure 24.—Stress relaxation of Ti-6Al-4V followed by unloading and recovery at 20 °C, showing proportional limit *PL* and range of threshold stress *Y*.

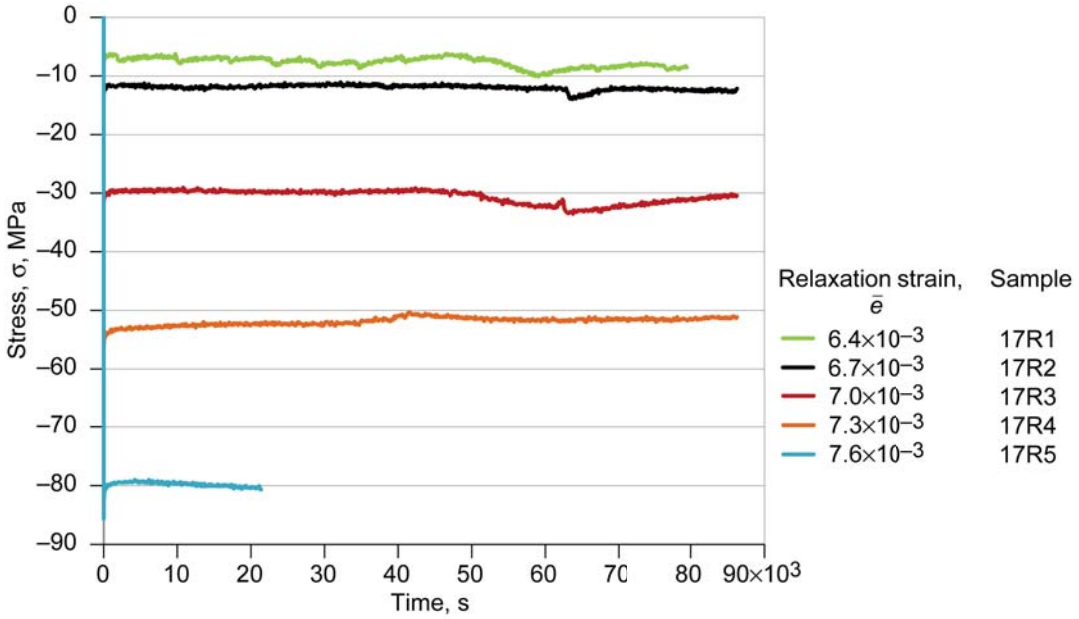

Figure 25.—Stress recovery at zero strain of Ti-6Al-4V following relaxation tests at 20 °C.

Determination of Key Viscoelastic Parameters at 427 °C

In this section, the procedure for determining the key viscoelastic properties of an alloy will be elucidated using actual results from sample 25, tested at 427 °C. As stated previously, the first step is to estimate the value of the threshold between reversible and irreversible behavior. Since *Y* is initially unknown, a good starting point is to keep the stress value of either creep or relaxation below 1/3 to 1/2 of the *PL* obtained from the slowest strain rate tensile test at the desired temperature. These low stress values should ensure that the test remains in the reversible regime. However, resolution is often poor in this range, and the linear region is small. If one remains within the reversible domain, multiple tests can be conducted without altering the material state, thus enabling efficient utilization of specimens in any viscoelastic test program. This of course is predicated on the assumption that all recovery times (in between tests) are sufficiently long to completely reverse any prior viscoelastic deformation. Consequently, we begin with the lowest stress level and progressively increase the stress level on subsequent tests to yield better data resolution.

The first test conducted under load control on sample 25 was a creep test (loaded at an equivalent strain rate of 0.001 s^{-1}) at 34 MPa, which should be clearly in the reversible regime since the *PL* for this sample at 427 °C is 476 MPa. It is observed in Figure 26 that creep behavior was exhibited during the 24-h hold at 34 MPa in the axial direction. Clearly, the specimen crept approximately 200 με before shutting down at approximately 40 000 s. The creep rate at the end of the hold period was 3.9×10^{-10} s^{-1}, while at the beginning it was 1.0×10^{-7}, a decrease of nearly 3 orders of magnitude. After unloading, the 24-h recovery period resulted in a return to near-zero strain. During the recovery phase, the strain recovers to a value of 50 με at 70 000 s, approximately 26 percent of its maximum. Note that in this and other figures, the time at the initiation of recovery (beginning of the unload) is typically reset to zero to facilitate display of the data. The recovery rate at the end of this test was -3.0×10^{-9} s^{-1}.

The next test on this sample was a stress relaxation experiment (loaded at a strain rate of 0.001 s^{-1}) performed at a total strain level of 430 με, again in the reversible regime (stress σ = 39 MPa and *PL* = 476 MPa, or 36 percent of the proportional limit). The strain versus time response is plotted in Figure 27 and clearly illustrates the excellent control of strain during the 24-h relaxation period. The recovery period (conducted under stress control subsequent to the stress being unloaded to zero) is also shown in this figure, indicating the strain recovers beyond zero and into the compression strain regime (i.e.,

–26 με). The recovery strain rate at the end of this test was -4.8×10^{-9} s^{-1}. The stress versus time response for this test is observed in Figure 28. The stress relaxes from a maximum value of 39 MPa and decreases until shutdown at 32.7 MPa, a 16 percent relaxation. The stress rate at the end of the relaxation period was -8.3×10^{-5} MPa/s. Note the curve denoted as recovery lies on the abscissae and illustrates the excellent ability to control stress at zero load during the 24-h recovery period. Clearly, Figures 27 and 28 are conjugates of one another (i.e., strain vs. time and stress vs. time, respectively).

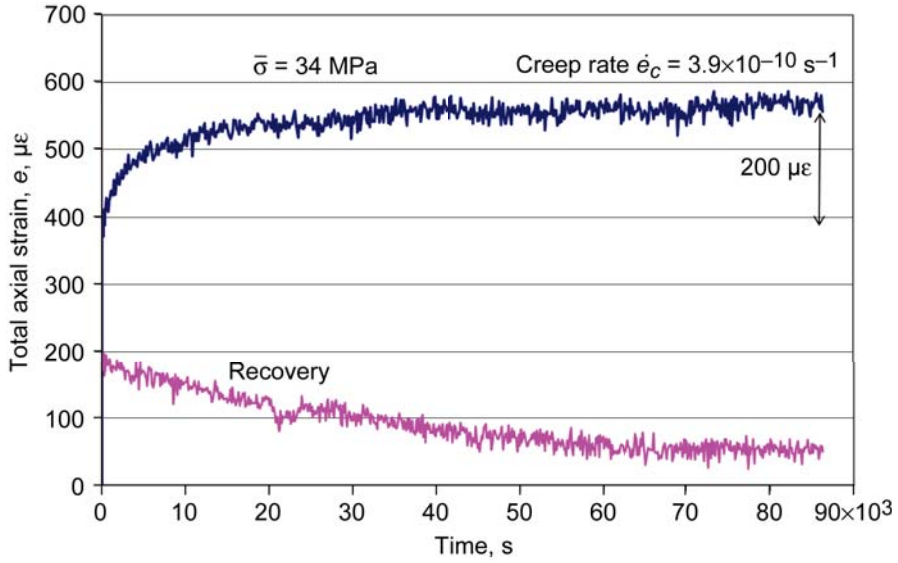

Figure 26.—Viscoelastic creep (stress $\bar{\sigma}$ = 34 MPa) and recovery ($\bar{\sigma}$ = 0 MPa) of Ti-6Al-4V in reversible regime at 427 °C (recovery rate = -3.0×10^{-9} s^{-1}).

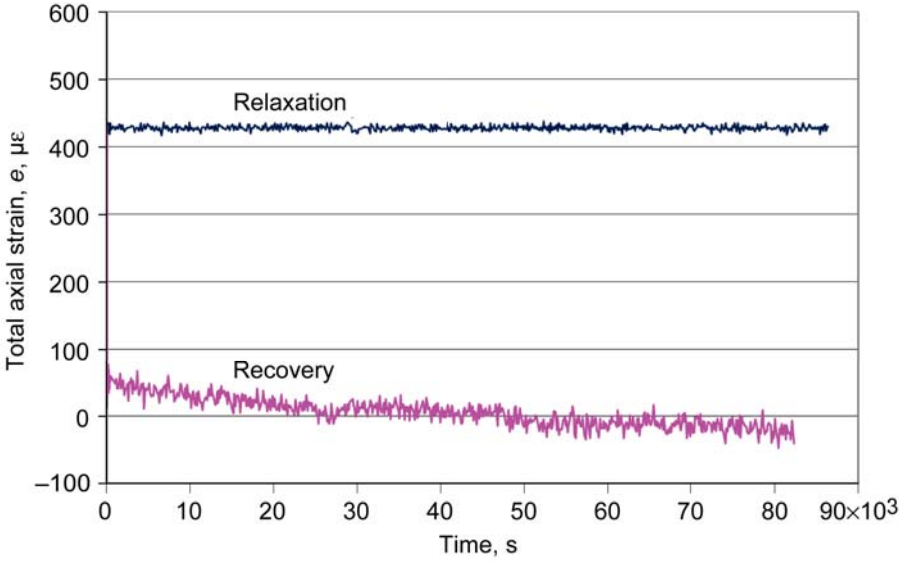

Figure 27.—Viscoelastic relaxation (strain $\bar{e}$ = 430 με) and recovery (stress $\bar{\sigma}$ = 0 MPa) of Ti-6Al-4V in reversible regime at 427 °C (recovery rate = -4.8×10^{-9} s^{-1}).

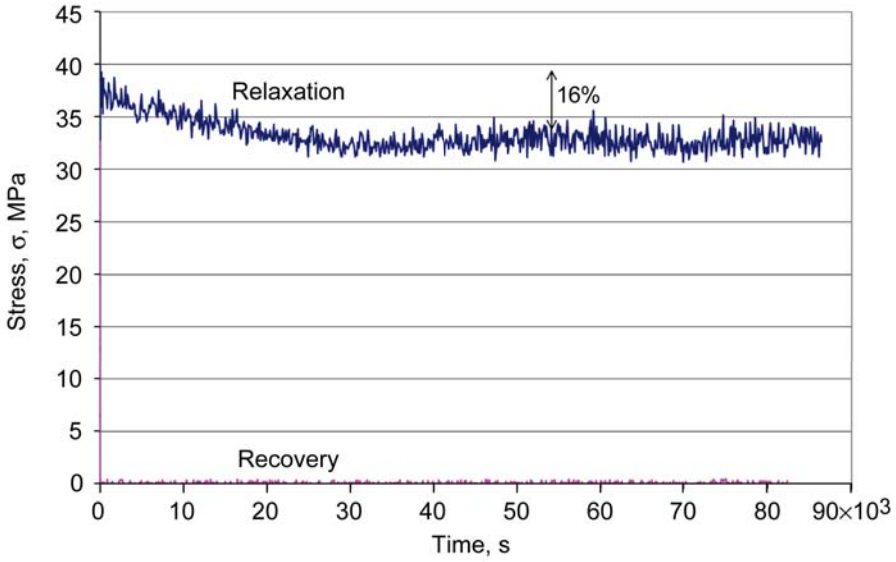

Figure 28.—Stress relaxation (strain $\bar{e}$ = 430 με) and recovery (stress $\bar{\sigma}$ = 0 MPa) of Ti-6Al-4V in reversible regime at 427 °C (final relaxation rate = -8.3×10^{-5} MPa/s).

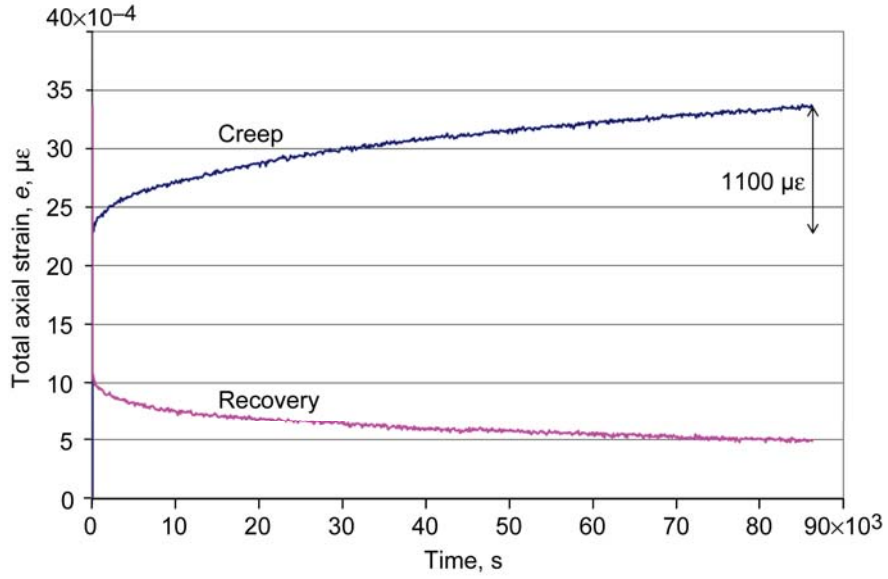

Figure 29.—Viscoelastic creep (stress $\bar{\sigma}$ = 206 MPa) and recovery ($\bar{\sigma}$ = 0 MPa) of Ti-6Al-4V in irreversible regime at 427 °C (creep rate $\dot{e}_c = 6.0\times10^{-9}$ s^{-1} and recovery rate = -2.3×10^{-9} s^{-1}).

The third test of this series is a creep test at a stress of 206 MPa (equal to 43 percent of the *PL*), which will be shown subsequently to be above the threshold and in the irreversible regime. The test exhibits substantial creep (Fig. 29) during a 24-h hold (i.e., 1100 με). Both a primary and secondary creep regime are exhibited with no indication of shutdown over the 24-h creep period. The strain rate at the end of the creep period is 6.0×10^{-9} s^{-1}. It is important to remember that the hold period for either creep or relaxation above *Y* needs to equal or exceed the hold period used in the recovery regime. This ensures that all reversible time dependence will be equally dissipated before the test is stopped. The unloaded sample recovers (at zero stress) to 500 με over a 24-h period, and reached a strain rate of -2.3×10^{-9} s^{-1} at the end of the recovery period. The strain does not appear to extrapolate to zero in any reasonable timeframe greater than 24 h. Note the amount of signal noise is significantly reduced at this load level in comparison

to the previous load levels. The conjugate curves illustrating the transverse strain behavior are described in Appendix B. Transverse strain was measured during most tests, and Poisson's ratio was usually calculated from it. These are both discriminating variables in comparing models because they are often more sensitive to minute changes in deformation.

Viscoelastic Parameters

The E_S can be established from calculating the secant modulus at saturation (i.e., once the response variable—be it strain or stress—has shut down) from a single reversible creep or relaxation test. However, it is always better to have a series of creep and stress relaxation tests that were conducted at various levels in the reversible regime. Both types of tests should be held for at least 24 h (this maximum time may be material dependent) to allow the controlling viscous mechanism time to dissipate. Note as temperature increases or for different materials the hold time period may have to be increased to ensure that sufficient dissipation occurs. Multiple tests enable one to account for associated uncertainties. Figure 30 depicts two relaxation tests and one creep test (two discussed previously) at 427 °C. The loading rate in each case was either 0.001 s^{-1} or its load equivalent during the creep test. The points at which the viscous mechanisms dissipate are denoted on the figure. A best-fit line through those points yields a secant stiffness of 68.8 GPa. This represents the time-independent stiffness E_S of this sample under the given test conditions. There is a small amount of scatter in the dissipation points, and this is typical when executing these types of tests. In fact, it was observed that whichever type of test was conducted first (for this sample it was creep) gave the most time-dependent deformation, resulting in the lowest single point value for E_S. Six out of seven samples showed this behavior. For the purposes of this report, all dissipation points were used, and an average E_S was calculated. Therefore, the use of more points (more tests) would improve the confidence of the estimation of E_S, but this would be accomplished at the cost of additional days of testing time (typically 2 days per test including the recovery). The difference in the calculated E_S using individual dissipation points rather than an average of all is what led to the range of upper strain values $\varepsilon_{\max}^{R}$ given in Figures 13 and 17.

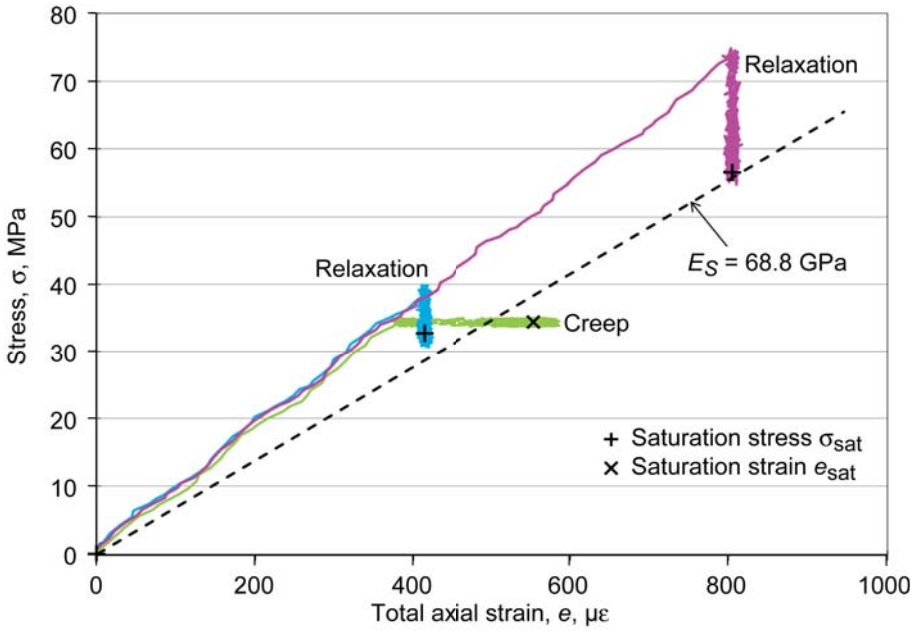

Figure 30.—Methodology for determining the infinitely slow modulus E_S of Ti-6Al-4V at 427 °C.

Utilizing the concept of viscoelastic subtraction (Ref. 2), the threshold value *Y*, delineating reversible and irreversible regimes, can be explicitly calculated using Equation (1). This is shown graphically in Figure 31, where the reversible and irreversible tests from sample 25 are now combined. The value of $\bar{\sigma}$ is 206 MPa, and ε^{IR} is 0.0005. Using E_S = 68.8 GPa, Equation (1) gives a value of 171 MPa for *Y*. Note the viscoelastic subtraction concept was derived using the idea of similar triangles; thus tests conducted in the irreversible region must be above *Y* and below *PL* (i.e., is applicable only in the linear region of stress-strain curves). The *PL* for this specimen (no. 25) is given in Table IV as 476 MPa. This indicates that there can be extensive irreversible deformation at stresses below the apparent "yield" point.

This above procedure was repeated for each specimen over the full temperature range of interest to yield E_S and *Y* as a function of temperature. These values are listed in Table IV. Both E_S and *Y* are plotted as a function of temperature *T* in Figure 32; the homologous temperature T/T_m is also shown (where T_m is the melting point), taken to be 1704 °C (1977 K). The longitudinal dynamic modulus E_D defined in Equation (3) and plotted in Figures 4 and 6 is also plotted and represents the highest modulus achievable at a given temperature. Note that E_S is equivalent to E_D up to temperatures of 316 °C; consequently this temperature delineates the temperature below which rate-independent elasticity applies. Above this temperature rate dependency becomes active and the infinitely slow modulus E_S decreases at a faster rate than E_D. This can be more easily viewed in Figure 6, which also shows that E_S is much lower at any given temperature than the slowest practical strain rate static modulus. For example at a temperature of 538 °C and a strain rate of 6×10^{-07} s^{-1}, the static modulus is 63 GPa, whereas E_S, is only 30 GPa. In Figure 32 both the values for *Y* and *PL* for strain rates of 0.001 s^{-1} are shown to decrease with increasing temperature. At room temperature, *Y* and *PL* are almost identical (*Y* is approximately 95 percent of *PL*), whereas at 538 °C they are significantly different: *Y* is approximately 10 percent of *PL* (see last column in Table IV), and near zero stress. At temperatures above 538 °C, it is assumed that *Y* is either zero or so small as to be unmeasureable. The trend line for *Y* represents the delineation between the reversible and irreversible deformation regimes over the temperature range of interest. Figure 32 constitutes the deformation modeling map for the Ti-6-4 alloy and provides insight into the required modeling assumptions as a function of stress-temperature regimes. It is interesting to note that significant time dependence is observed at homologous temperatures (T/T_m) as low as 0.29 in this alloy, which is consistent with the range of values (0.25 to 0.30) normally cited for initial creep activity in most structural alloys.

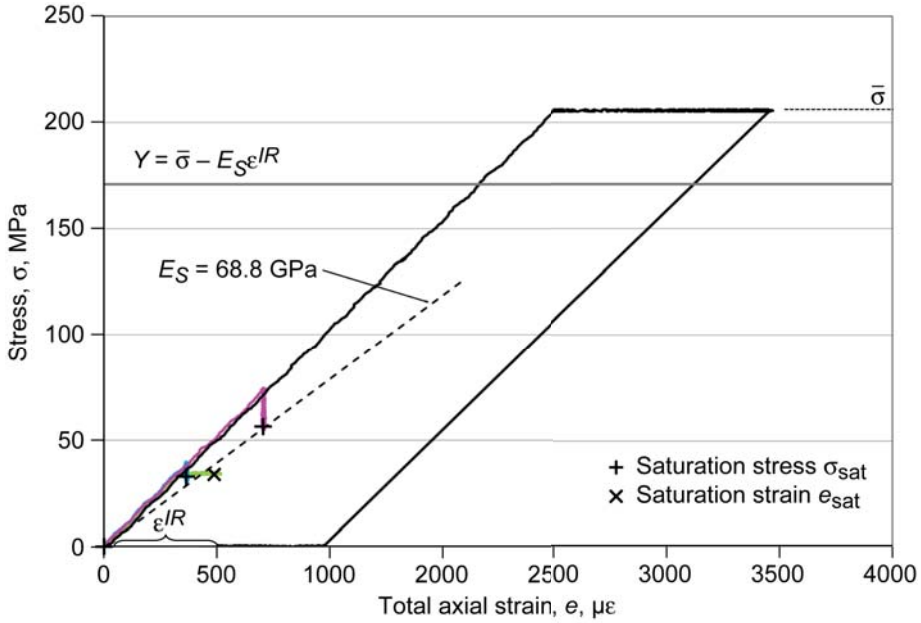

Figure 31.— Determination of reversibility threshold stress *Y* for Ti-6Al-4V at 427 °C, where E_S is infinitely slow modulus, $\bar{\sigma}$ is creep stress, and ε^{IR} is irreversible strain.

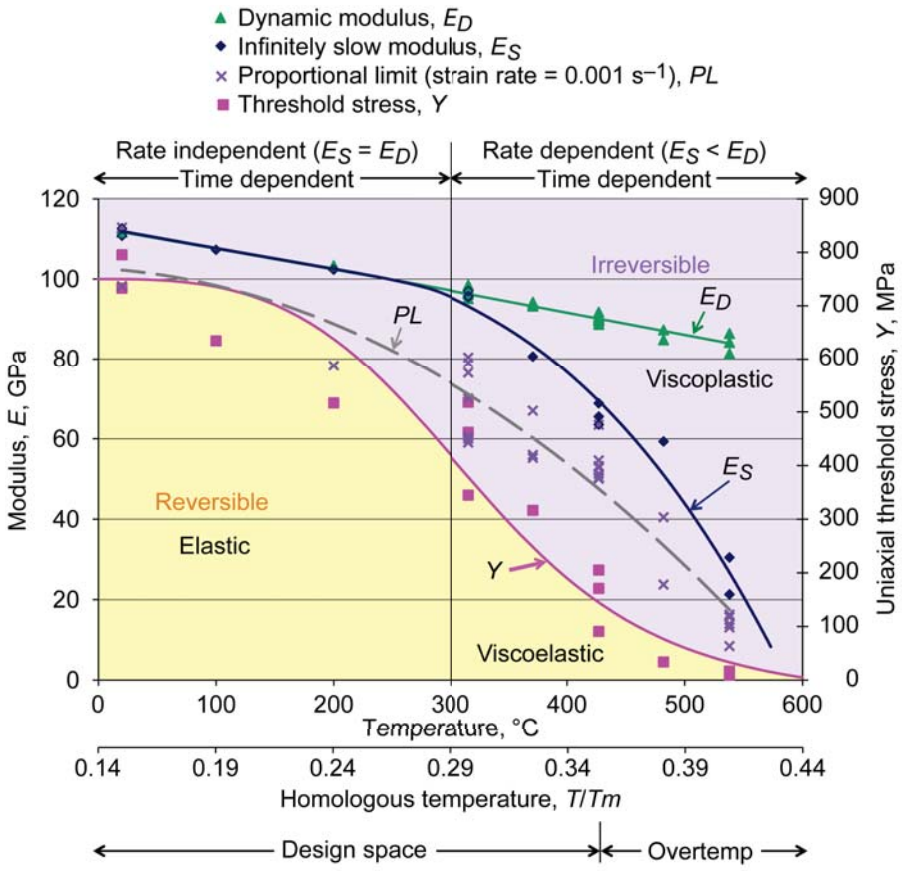

Figure 32.—Ti-6Al-4V time-dependent deformation modeling map.

Rate Effects

Ideally *Y* could be determined by obtaining the proportional limit of an infinitely slow strain rate tensile test. The question is what constitutes an infinitely slow tensile test? Based on the creep rate at complete dissipation for the test depicted in Figure 26, the imposed loading rate would need to be on the order of 3.9×10^{-10} s^{-1} at the temperature of 427 °C. This is significantly slower than a typical servohydraulic control limit of 6.0×10^{-7} s^{-1} and could not be achieved here in a tensile test. Figure 33 provides the proportional limits for a number of measurements made for very fast (0.001 s^{-1}) and very slow (6.0×10^{-7} s^{-1}) strain rates over the temperature range of interest. The trend line for *Y* determined using the viscoelastic subtraction method plotted in Figure 32 is included in this figure for comparison. Obviously, the fast-strain-rate proportional limits agree with the extracted values for *Y* up to approximately 316 °C, whereas they are significantly higher than the calculated *Y* values at higher temperatures. As noted before, as temperatures rise and stress levels fall, the noise level in the measurements become more problematic and make accurate determination of both *PL* and *Y* (since the determination of E_S is problematic as well) more difficult. It is noted in Figure 33 that the *PL* values at very slow strain rates are an excellent estimate for *Y*. Furthermore, these results strongly suggest a *PL* fraction rule that is 50 percent of the *PL* obtained from a very slow strain rate tensile test would be a good starting stress for the viscoelastic series. This estimate should ensure that a given test is within the reversible regime when conducting viscoelastic exploratory/characterization testing, regardless of the temperature.

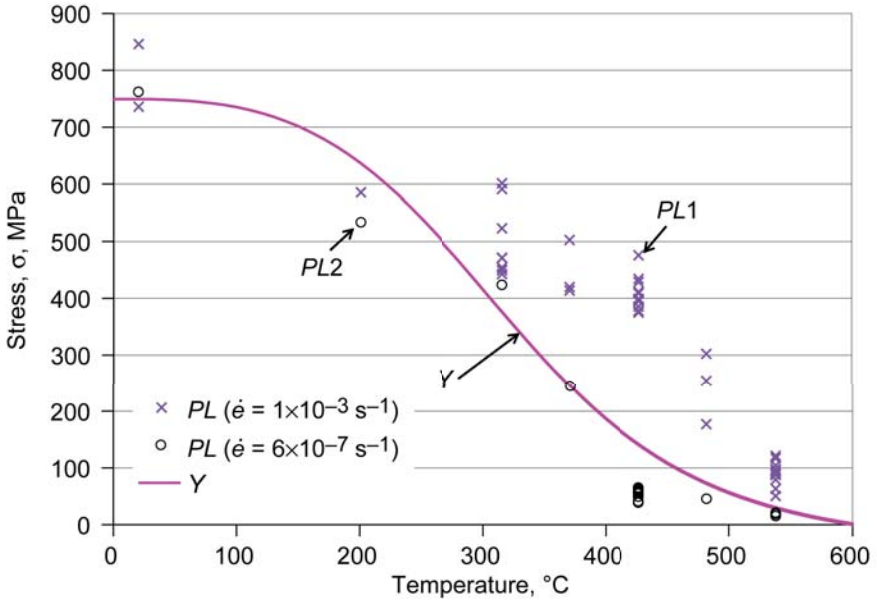

Figure 33.—Comparison of proportional limits at very fast (*PL*1) and very slow (*PL*2) strain rates $\dot{e}$ and threshold stress *Y* for Ti-6Al-4V at different temperatures.

Since viscoelastic subtraction uses a test above *Y*, but below the *PL*, and since the *PL* is a function of strain rate, one could ask what strain rate needs to be employed to calculate *Y*. In an attempt to ascertain this, *Y* was calculated on a sample (i.e., sample 26) using both very fast and very slow strain rates. The test sequence is shown in Figure 34. Tests R2 and C1 were conducted at a very slow strain rate (8×10^{-7} s^{-1}). All other tests were conducted at a very fast strain rate (0.001 s^{-1}). Moreover, the first three tests (relaxation) were conducted below the slow-rate *PL* of 55 MPa. The fourth test (creep) was conducted above the slow-rate *PL*, but still under the suspected *Y* value. The remaining two tests were conducted above *Y*, but below the fast-rate *PL* and appear to be "fully elastic" during loadup. The final creep value of 445 MPa is within the region of fast-rate *PL* values, which ranges from 375 to 476 MPa. The strain versus time behavior for these tests is depicted in Figure 34 along with the corresponding ε^R and $\varepsilon^R_{\max}$ associated with the deduced *Y* value of 199 MPa. Figure 34(a) shows that only the two highest stress creep tests fall above *Y* since the initial loadup strains exceed Y/E_D and the maximum accumulated strain after 24 h exceed $\varepsilon^R_{\max}$. The slower rate creep test (68 MPa), while still under the threshold value, does not show evidence of shutting down during creep and appears to exhibit a constant rate, which is in contrast to previous experience. Although this test depicts a final recovery strain of 110 με after the standard 24-h recovery period, continued testing showed that the recovery strain decreased further to 58 με after another 18 h and was still decreasing. Consequently, this suggests that for slow-strain-rate loading more than 24 h may be needed to reach saturation of the time-dependent processes, particularly at lower temperatures. Figure 35 documents the relaxation behavior of the first three tests, all taken to a strain limit of 0.0004. The relaxation behavior is essentially identical regardless of the loading rate. All three tests also saturate to approximately the same equilibrium stress level of 27.5 MPa, which provides a 68.75-GPa estimate for the infinitely slow modulus (i.e., $E_S = \sigma_{sat}/\bar{e}$). This indicates that deformation response under the threshold value is rate independent, as long as the test is maintained below the rate-dependent proportional limit.

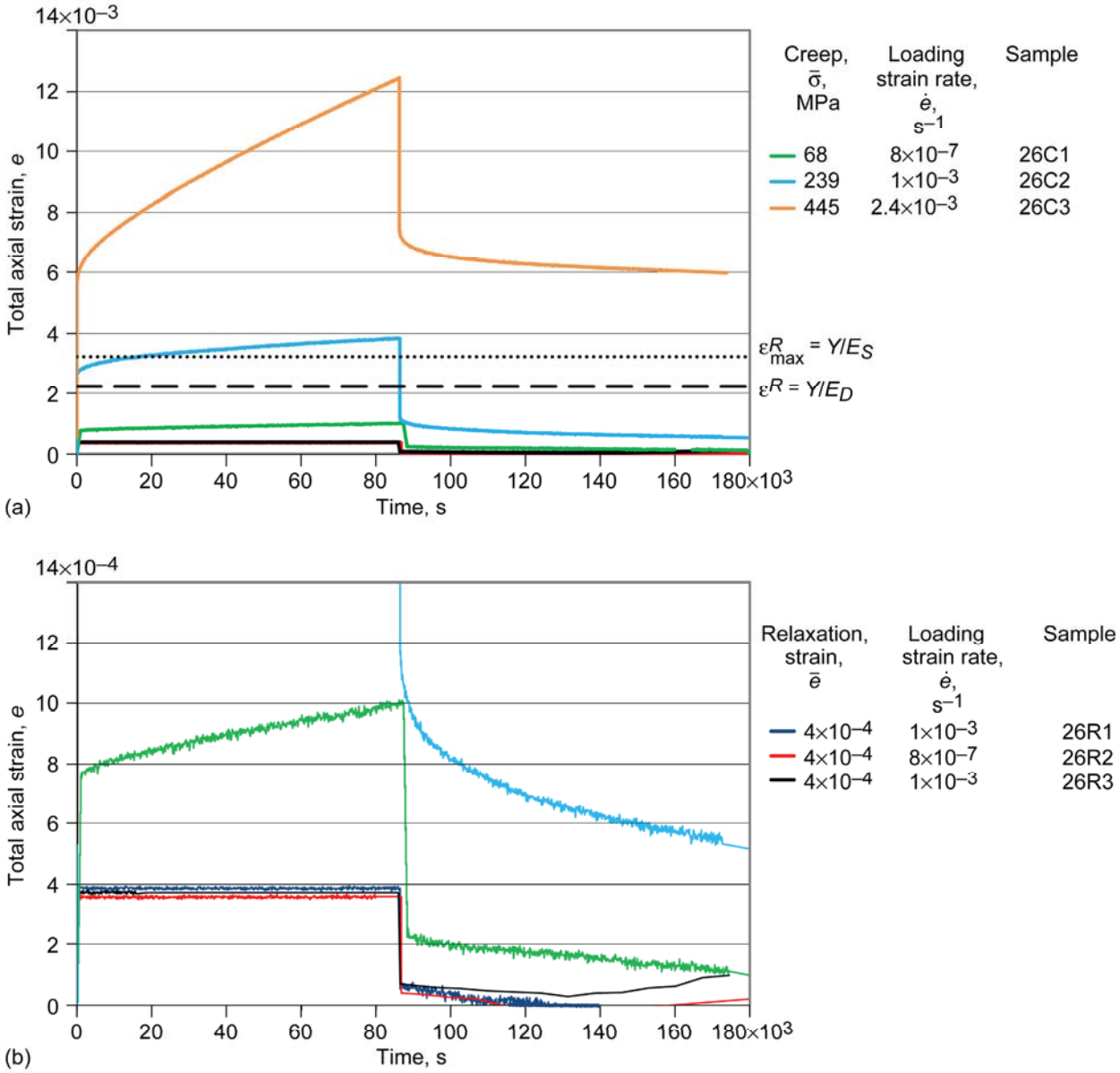

Figure 34.—Creep behavior of Ti-6Al-4V at 427 °C as function of loading strain rate $\dot{e}$, where ε^R_{max} is maximum reversible strain, ε^R is reversible strain, Y is threshold stress, E_S is infinitely slow modulus, and E_D is dynamic modulus. (a) Full-strain range. (b) Expanded view of low-strain range.

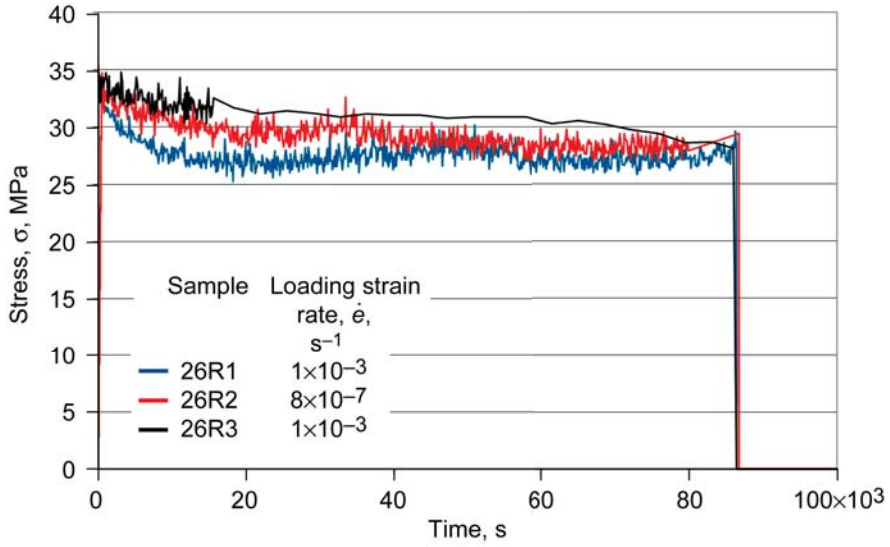

Figure 35.—Stress relaxation behavior for very slow and very fast loading strain rates $\dot{e}$ in the reversible regime.

History Dependence of the Threshold

In order to investigate the effect of prior deformation on the threshold value, a test (sample 83) was conducted in which *Y* was first established, a large viscoplastic deformation was then applied, and the threshold was again determined. Figure 36 displays the stress-strain response at 427 °C for this test series. The dotted lines represent the data from probes on samples with no permanent deformation, whereas the solid lines show data from the probes after large sample deformation. All of the tests conducted in this series were creep with two tests below the threshold and one slightly above to determine *Y*. The large-scale deformation test was crept at 577 MPa, which is both above the threshold and also above the 0.2 percent yield point (552 MPa) of this sample. This creep test achieved a total strain of 4.8 percent before it was unloaded and recovered at zero load.

The strain versus time diagram is given in Figure 37 with dotted lines again depicting the initial probes. This chart shows that the before and after creep responses are similar, with the initial response being slightly higher than the final response at the lowest load, the same at the medium load, and slightly below at the highest load above *Y*. It should also be noted that the strain during recovery for both sets of below-*Y* tests ended near zero strain. In both load cases the post-yield tests recovered to slightly lower strains than the pre-yield tests, but this is assumed to be due to experimental scatter. However, the tests for the above-*Y* loads exhibited similar behavior in that the post-yield test also recovered to slightly lower values. The viscoelastic parameters were calculated from this test series and are shown in Table V.

Although both the infinitely slow modulus E_S and *Y* are similar for both pre- and post-yield tests, the values after yielding are slightly higher. However, both sets fall in the range of the viscoelastic parameters given in Table IV. The last row under the 427 °C test in Table V lists a second *Y* value calculated by using the original value of E_S, 74 GPa. Using this value for the stiffness makes little difference in the resulting threshold values.

An additional test series (7C) was conducted at 427 °C on a sample that had prior creep deformation at 552 MPa (past the 0.2 percent yield stress), followed by recovery. Several creep tests were subsequently performed to determine the post-yield viscoelastic parameters. The modulus E_S was calculated to be 78 GPa and threshold *Y*, 235 MPa. These values are again just slightly outside (<5 percent) the range of those given in Table IV.

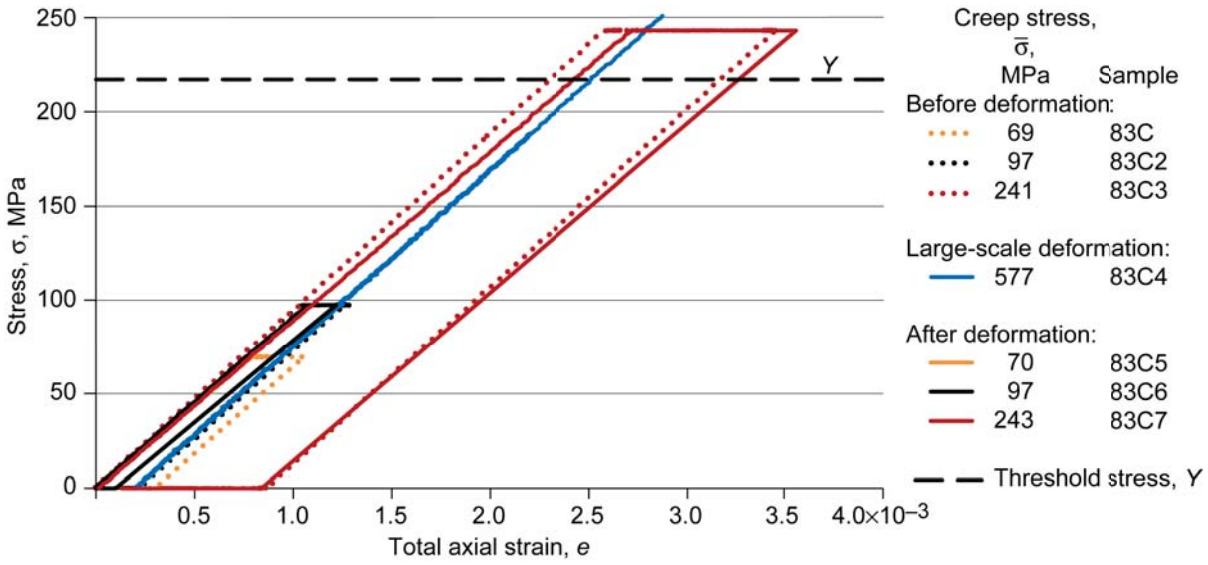

Figure 36.—Threshold stress *Y* for Ti-6Al-4V at 427 °C before and after large-scale deformation.

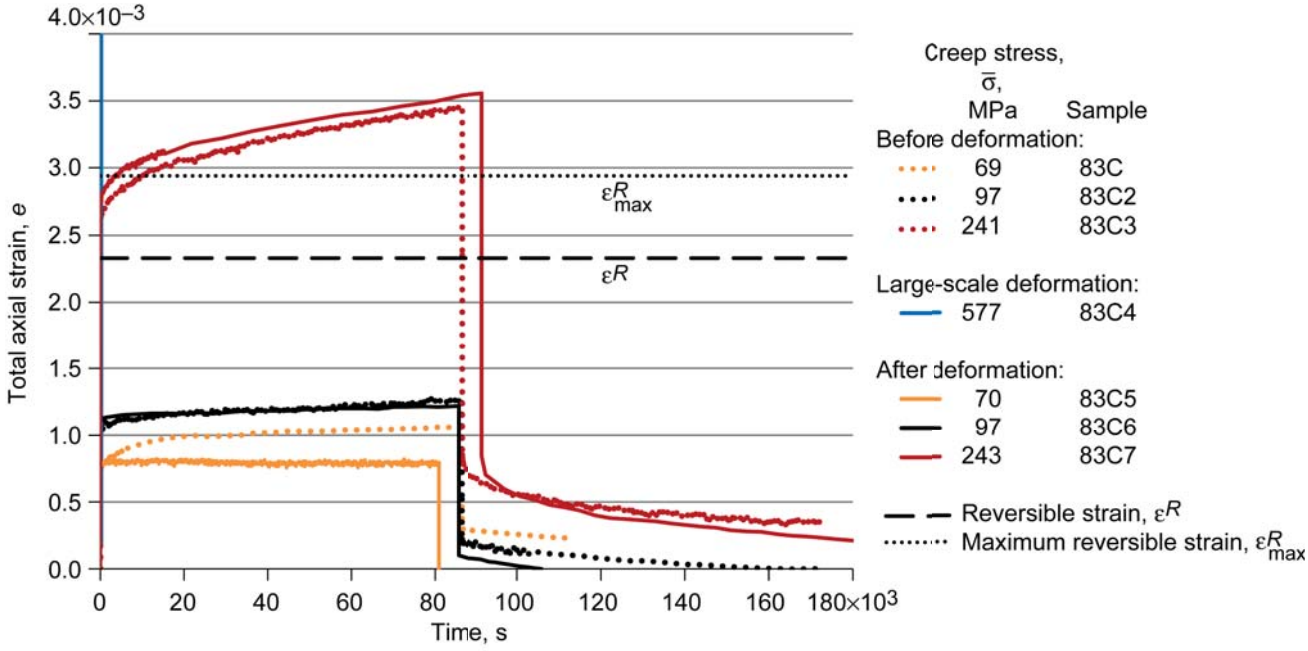

Figure 37.—Creep response for Ti-6Al-4V at 427 °C before and after large-scale deformation.

Finally, a test was conducted at 538 °C with pre- and post-yield viscoelastic probes. A tensile test to 502 MPa (1.8 percent strain) with subsequent unloading and recovery was performed between the probes to induce large-scale deformation. The viscoelastic parameters are given in Table V and show that the tensile deformation has no effect on the stiffness E_S. There was a decrease in the value of the threshold. Again all values fall in the range of those listed in Table IV for tests at 538 °C. Hence, it is reasonable to assume that the viscoelastic parameters are minimally influenced by inelastic flow. Further given that the threshold value, *Y*, is unaffected by inelastic flow (i.e., no isotropic hardening) this material can also be idealized by a kinematic hardening formulation consistent with Saleeb and Arnold (Ref. 1).

TABLE V.—PRE- AND POST-YIELD EFFECT ON VISCOELASTIC PARAMETERS FOR Ti-6Al-4V

	Infinitely slow modulus, E_S, GPa	Difference, percent	Threshold stress, Y, MPa	Difference, percent
427 °C				
Pre-yield	74		217	
Post-yield	81	9.7	226	3.9
Using E_S = 74			227	4.6
538 °C				
Pre-yield	21		17	
Post-yield	21	0.0	14	–12.4

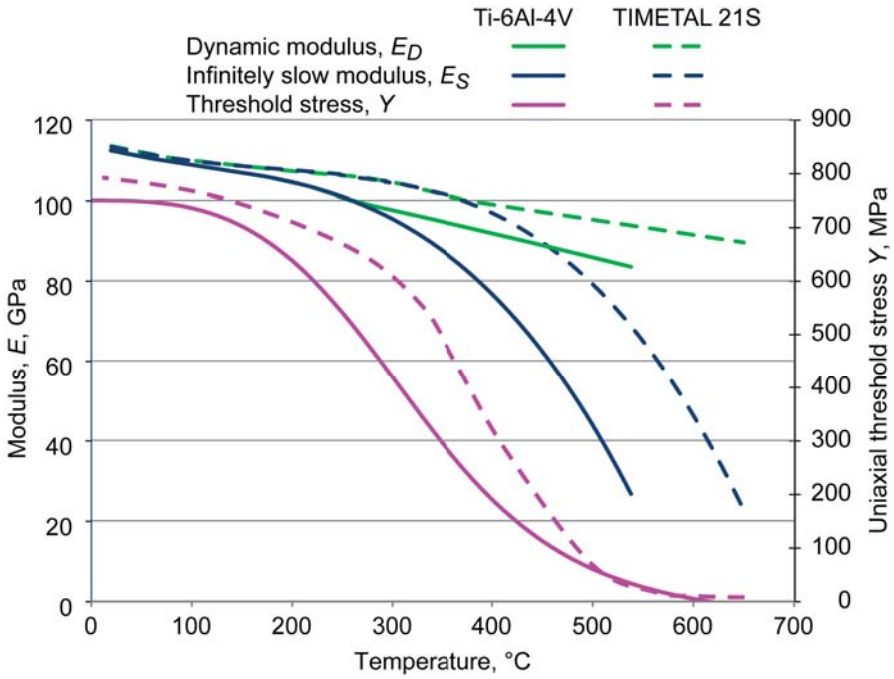

Figure 38.—Comparison of viscoelastic parameters of Ti-6Al-4V and TIMETAL 21S (Refs. 2 to 4).

Comparison With TIMETAL 21S

Since it has been shown that Ti-6-4 displays viscoelastic behavior, it will be compared to what was observed for TIMETAL 21S (Refs. 1 and 2). The data from these past programs were reevaluated and plotted along with Ti-6-4 on the deformation modeling map shown in Figure 38. Both alloys show similar behavior with the TIMETAL 21S showing better properties at higher temperatures. This is to be expected since TIMETAL 21S was developed to be used at higher temperatures (Ref. 22) and to have creep resistance equivalent to Ti-6-4. TIMETAL 21S exhibits a higher threshold stress than Ti-6-4. Although they appear in Figure 38 to have identical thresholds at 500 °C and above, this is just a resolution issue. TIMETAL 21S actually has a threshold at 500 °C, which is 5 to 6 times that of Ti-6-4. Both the dynamic modulus (E_D) and the time-independent modulus (E_S) for TIMETAL 21S are also larger than Ti-6-4. Furthermore, the delineation between rate dependency and rate independency is over 100 °C greater for TIMETAL 21S than for Ti-6-4.

Discussion

Whereas the basic information required for characterizing the viscoelastic model put forth by Saleeb and Arnold (Ref. 1) employs testing of a basic nature (e.g., tension, creep, and stress relaxation), acquiring the required data necessitates a more difficult test protocol involving unloads with long hold times. The stress levels at which most of the tests are performed are low, with both the stress and strains being near the noise floor of the equipment. This becomes more evident at higher test temperatures, which unfortunately is the regime of interest where viscoelastic deformation dominates. For example, at 538 °C there is a 75-percent decrease in the stress because of viscoelastic relaxation, whereas at 316 °C there is only a 3-percent decrease. Additionally, the stress levels at 538 °C (16 MPa) are obviously much lower than those attained at 316 °C (280 MPa). Hence, electronic and thermal noise, as well as test rig stability, is critical to the success of these tests. Similarly, small load offsets typical of loading and gripping samples must be minimized, or they could result in stresses occurring above the threshold levels. Also, when control-mode switches are utilized, they must occur smoothly (no bumps in stress or strain) in order to prevent overshooting of the desired value and landing in the irreversible range. These factors make the conducting of seemingly simple tests more difficult.

It should be reminded that each step of the viscoelastic tests requires a minimum of 2 days to complete: the first 24 h in the loading stage and the second 24 h in the recovery phase. This timeframe is convenient for testing because changes do not occur in the middle of the night. Also, 24 h is sufficiently long to cover any time-dependent behavior that may be experienced in aeronautical applications. For materials used in power generation, deep-space probes, or other long time-at-temperature applications, this dwell time may have to be revisited. Obviously, the hold times in these phases can be reduced, but are done so at the risk of errors in the conclusions. In both phases the deformation mechanisms are required to fully dissipate, and this requires a certain timeframe. This study has shown that more time is required for the viscoelastic mechanisms to dissipate or completely recover at higher temperatures than at lower temperatures. Results suggest that 24 h is not quite sufficient at 538 °C for the creep process to completely dissipate. However, at 316 °C, the process can dissipate in 6 h. Hence, variable hold times could be employed to minimize overall test times. Unfortunately, the required hold times are not only temperature dependent, but also material dependent. Therefore, advanced knowledge of the material behavior is required to effectively minimize test times, and this is most likely resolved through a series of screening tests, possibly negating any time-saving advantage associated with modifying the dwell times.

To calculate the viscoelastic constants E_S and Y, there are theoretically only three tests required at any given temperature. Two of these are conducted below Y in the reversible regime. The last test is conducted above Y in the irreversible regime, but below PL. These three tests can all be performed on the same sample, since the deformation resulting during the first two experiments—conducted within the reversible domain—is fully recovered. In fact, it is advised that they all be performed on one sample to eliminate specimen-to-specimen scatter in the results. The basic test procedure is shown in Figures 5, 30, and 31. The tests below Y consist of a combination of creep and relaxation tests. They can be both the same type of test, or can be different (one creep and one relaxation test). The preferred test above Y is a creep experiment, since viscoelastic subtraction requires explicit measurement of the irreversible strain accumulated after all recovery is achieved. This is most easily obtained from a creep test, although a stress relaxation experiment could also be used.

Although only three tests (see Fig. 5) are necessary for establishing the viscoelastic parameters, practice usually requires more testing. More tests conducted below Y provide additional points enabling better linear regression fits of E_S. The results indicate that the first test conducted, and all others like it, seems to yield the lowest value of E_S in a sample (see Fig. 30), suggesting it is prudent to get additional points from both types of tests. Moreover, it is often difficult to determine if dissipation or full recovery has occurred, and more tests can aid in this determination. Part of the difficulty of determining this is that the deformation behavior, particularly at low stress values, can be influenced by specimen-specific history, such as residual stresses (in part due to machining), local microstructure variations, surface roughness, and specific temperature variations, to name a few. These may lead to odd deformation

behavior such as negative creep; recovery shutdown at nominal, nonzero values; recovery into the negative strain regimes; and recovery as increasing rather than decreasing values. Again these effects are more readily overcome at lower temperatures where the values of both *Y* and *PL* are high and are high enough that most of these effects become nonissues. However, the viscoelastic effects are once again more important at the higher temperatures. Nonetheless, a reasonable amount of testing to yield accurate results per temperature is four tests, resulting in a total of 8 test days per sample.

Even though the final viscoelastic test is above *Y* and the specimen does incur some irreversible deformation, the stress levels are still below those of the proportional limit. Hence the specimen contains comparatively little permanent deformation and may be used for subsequent high-strain (viscoplastic (post-yield) or damage) testing. Given that the sample contains prior history, the researcher must determine whether this is important to subsequent testing or not. All of the samples used in this study were used for further viscoplastic tests. The determination of whether or not the prior viscoelastic history was important was made only after high-strain tests were conducted on virgin samples and were available for comparison. Experience would suggest that these viscoelastic specimens can at a minimum be used to obtain initial estimates of monotonic tensile behavior at a given strain rate to failure.

Two key events determining the success of these tests is the dissipation of viscoelastic deformation and the complete reversibility of the deformation during unloading and recovery. Since these determinations are complicated by the aforementioned problems, some guidance will now be given. Complete dissipation is theoretically defined by an instantaneous slope of zero for the response variable (stress or strain). It was determined that creep rates of less than 6.0×10^{-09} s^{-1} were sufficient to declare that the mechanisms had dissipated. Similarly, relaxation rates of less than 3.3×10^{-04} MPa/s were required. Recovery was always based upon a strain proximity to zero rather than a rate. Experience showed that recovery values within 0 ± 100 με were suitable to account for experimental error. If the recovered strain was larger than this, the test was declared to have been in the irreversible regime. Although this process was tempered with any subsequent experiments per the aforementioned discussion on repeat tests below *Y*. The observed strain rate at the end of recovery ranged between -5.0×10^{-9} and -3.8×10^{-10} s^{-1}.

The biggest factor in identifying reversibility of a test is whether there is a secondary creep rate (nonzero rate) or not. This poses the question at what creep rate can the test be considered to be zero? The strain rates during dissipation (i.e., loading portion of test) were found to be between 1.0×10^{-10} and 6.0×10^{-9} s^{-1}, whereas the strain rates at the end of the recovery portion of the test in the reversible regime were between -3.8×10^{-10} and -5.0×10^{-9} s^{-1}. It is interesting that the strain rates during dissipation in the reversible regime were very similar (ignoring the sign) to the final recovery rates. Above *Y*, the final creep rate was always larger than the final recovery rate. There were few tests conducted around the proportional limit to draw conclusions about rates in this regime. Given these observations, one could conclude that a creep rate smaller than 1.0×10^{-9} s^{-1} indicates fully dissipated mechanisms (i.e., zero secondary creep rate), and would seem to indicate reversibility.

Stress relaxation tests tended to dissipate with stress rates between -3.8×10^{-5} and -3.3×10^{-4} MPa/s in the reversible regime. There were too few tests conducted above *Y* and below the proportional limit to compare stress rates in the irreversible regime. These results show that judging dissipation is subjective, particularly without a series of like tests centered around *Y*. The best judge of whether or not the test fell into the reversible regime is to ensure that the axial recovery strain returned to a near-zero value. Even here, multiple tests make this decision easier.

Traditional metallic behavior assumes that inelastic behavior (flow) at room temperature does not occur until the applied stress exceeds the yield point. Time-dependent deformation behavior at room temperature below the yield point in titanium alloys, especially in Ti-6-4, is not new and has been documented previously (Refs. 12 to 17). In the majority of these cases, the authors used a 0.2-percent offset as their yield point definition. However, the current work shows that time-dependent deformation is possible at values far below this point. For example, *PL* at 20 °C for the sample represented in Figure 20 (no. 17) is given in Table IV as 737 MPa. Yet this sample has significant time-dependent behavior (see

Figs. 21 and 22) below the proportional limit at a stress of 690 MPa. Wapniarsky, Rotem, and Rosen (Ref. 13) performed creep tests at room temperature on annealed Ti-6-4 at stresses as low as 85 percent of the 0.2-percent yield (904 MPa) and showed evidence of time dependency. Although this stress level is in the range of Y values observed here, it is unknown whether or not Wapniarsky's levels were above the threshold of those particular samples. Wapniarsky does state that the observed creep is transient at all the stress levels investigated, and they exhibited only a primary creep regime followed by eventual shutdown. At least some of their applied stress levels were above Y, and still complete dissipation was observed, implying that a few of these tests were in the irreversible regime. The authors did not unload and recover the samples, so it cannot be definitively known which of the tests, if any, were reversible, since full dissipation alone is not a sufficient criterion at low temperatures to define reversibility. It should also be noted that because of the very long time periods (2000 h) necessary to achieve full dissipation, a very long clock would be required in the GVIPS model.

Lastly, the reader is reminded that when dealing with elevated-temperature response, understanding rate dependence is essential. Figure 6 shows the modulus as a function of strain rate and temperature. For specimens conducted at fast rates (e.g., 1×10^{-4} to 1×10^{-3} s^{-1}) the moduli are nearly identical to those conducted under dynamic conditions. Thus the loading rates of 0.001 s^{-1} used in most of the viscoelastic testing was sufficient to lock in practically all material-time dependency. Only at temperatures of 482 °C and above did the fast-rate static modulus deviate from the dynamic modulus, where the strain rate from the dynamic modulus tests is approximately 3 orders of magnitude larger than the fastest static strain rate. Although this implies that the applied static rates still should have been faster, we feel that the difference between the curves was negligible. Moreover, faster rates would have decreased the ability to properly control the tests. Clearly, lower loading rates, certainly less than 1×10^{-4} s^{-1}, would have allowed some of the time-dependent behavior to be released as the sample was loaded. Obviously, the desired loading rate is both temperature and material dependent. There may be some materials for which no realistically achievable rate can totally lock in all time dependency. Additionally, there may be other materials where any realistic load rate is sufficient to lock in time dependency.

Sinha (Ref. 23) investigated the relaxation behavior of Ti-6Al-2Sn-4Zr-6Mo to describe its viscous strain behavior. For fast loading rates between 1×10^{-3} and 1×10^{-2} s^{-1}, he found that the static modulus also agreed with the values from dynamic tests. Sinha and Kearsey (Ref. 24) documented the same finding on a nickel-base superalloy, IN–738LC. They suggested that because of the fast loading rates that "inelastic strain was not introduced during loading." Actually, inelastic strain is indeed being incurred during this time in spite of the observed linear stress-strain response (apparent elastic behavior). It is this "locked-in strain" that manifests itself as viscoelastic behavior during subsequent creep or relaxation. During Sinha and Kearsey's tests, samples were unloaded to zero load and allowed to recover for up to 1000 s. Viscoelastic recovery (termed by Sinha and Kearsey as "delayed elastic strain") was observed in each case, but did not return to zero strain. Relaxation and creep tests showed the absence of a full dissipation of mechanisms in stress and strain, respectively, during the loading portion of the tests. This indicates that either all of the tests had been loaded into the irreversible regime and none of them were at loads below the threshold or (most likely) that the hold times were far too short. The current work indicates that significantly longer times are required to allow all time-dependent behavior to cease. Sinha (Ref. 23) did indicate that the recoverable strain had been recognized to be a significant portion of the total strain at high temperatures. He also implied (Ref. 25) that time dependency may occur below a threshold, where threshold was defined as an internal or back stress. Therefore, the time-dependent reversible and irreversible response and modeling approach used for Ti-6Al-4V could be applicable to many nickel-base superalloys.

Summary of Results

The time and rate dependence of deformation in both the reversible and irreversible regimes were investigated and documented for annealed Ti-6Al-4V. A series of tensile, creep, and stress relaxation tests was conducted from 20 to 538 °C. Unloading followed by a recovery period was performed at the end of each test. These tests were in support of characterization of the GVIPS (generalized viscoplasticity with potential structure) viscoelastoplastic constitutive model, which will be used in damage prognosis for aircraft engines. The salient features of this work are

(1) The modulus was found to be rate dependent, particularly above 316 °C. It was bounded by stiffness limits: the dynamic modulus E_D at very fast rates (upper limit) and the modulus E_S at infinitely slow rates (lower limit).
(2) This material was found to be viscoelastic at low stresses over the entire range of test temperatures based on the following observations:
   (a) At stresses much below the value of the proportional limit (*PL*) the material exhibited time dependency that completely dissipated given sufficient time.
   (b) Upon unloading to zero load, the strains recovered to zero in a viscous fashion.
   (c) There was an experimentally derived stress below which the material deformed by reversible mechanisms and above which it deformed by irreversible mechanisms. This stress threshold is referred to in the model as *Y*.
   (d) Viscoelastic strain was shown to be a significant portion of total strain at elevated temperatures.
   (e) The value for *Y* was low and a small proportion (10 percent) of the fast-rate *PL* at high temperatures and a large fraction of *PL* (99 percent) at low temperatures.
(3) Below the threshold, primary creep eventually dissipated, with final creep rates being less than 6×10^{-9} s^{-1}.
(4) Above the threshold, creep tests transitioned from primary to secondary creep regimes.
(5) Time-dependent deformation, although extremely small, was observed at temperatures as low as 20 °C and existed both below *PL* and *Y*.
(6) The experimental results substantiate the fundamental assumptions of the viscoelastic portion of the GVIPS model.

Conclusions

In conclusion, there can be substantial amounts of time-dependent reversible and irreversible deformation below the proportional limit (or traditionally defined yield points), of this material and over the entire range of temperatures studied. The irreversible or permanent deformation occurs above a threshold stress, which can be found experimentally. Below this threshold, all deformation is reversible. This threshold was found to be invariant of the loading rate. The deformation types can be displayed in a deformation-modeling map, which shows the active mechanisms in each regime and the key viscoelastic partitioning parameters—the dynamic modulus (E_D), the modulus at infinitely slow rate (E_S), and the uniaxial threshold stress (Y)—as a function of temperature. These parameters were found to decrease with increasing temperature. Moreover, the modulus decreased with strain rate at high temperatures, reaching a lower limit at the calculated value E_S, which represents the infinitely slow strain rate. The viscoelastic parameters E_S and Y do not appear to be affected by prior deformation in this material, thus suggesting that this material can be idealized using a kinematic hardening formulation.

Finally, the data presented herein will be used for characterizing the viscoelastic portion of the GVIPS (generalized viscoplasticity with potential structure) model and documenting the ability of the model to describe the viscoelastic behavior of Ti-6Al-4V. Similar experimental and modeling publications will also follow that characterize the viscoplastic and damage behavior of Ti-6Al-4V and include predictions of complex deformation behavior.

Appendix A—Symbols

e	total axial strain
e_c	axial creep strain
e_{sat}	saturation strain
e_t	transverse strain
$\overline{e}$	relaxation strain (applied strain level)
$\dot{e}$	loading strain rate
$\dot{e}_c$	creep rate
E	static modulus
E_D	dynamic modulus
E_m	Maxwell spring stiffness
E_S	infinitely slow modulus
PL	proportional limit
T	temperature
T_m	melting point
Y	uniaxial threshold stress
ε^{IR}	irreversible strain after achieving full recovery
ε^{R}	reversible strain
ε^{R}_{max}	maximum reversible strain
η	dashpot viscosity
κ	threshold stress in shear
ρ	relaxation time
ν	Poisson's ratio
σ	stress
σ_{sat}	saturation stress
$\sigma_{0.02\%}$	0.02 percent yield point
$\sigma_{0.2\%}$	0.2 percent yield point
$\overline{\sigma}$	applied stress level

Appendix B—Transverse Strain Behavior

The viscoelastic model put forward by Saleeb and Arnold (Ref. 1) assumes that all moduli (i.e., E_s, E_m, and n) are coincident, which implies time independency of Poisson's ratio. Consequently, in this study an attempt to experimentally assess the time dependency of Poisson's ratio was made. Previous attempts at this were inconclusive because the contacting diametral extensometer was found to creep into the sample over time yielding erroneous values (Ref. 2). For this reason, a noncontacting, optical extensometer was chosen specifically for this test program on Ti-6Al-4V (Ti-6-4). Transverse (or diametral) strain data were collected on nearly every test.

The results from the transverse strains were less than ideal because of a number of factors. First, the practical resolution of the optical micrometer was not adequate for the low strain levels observed in the viscoelastic tests. At 538 °C a resolution of 0.002 mm could be resolved, which equates to a transverse strain of 300 με. Given an estimate of the Poisson's ratio of 0.3, this resolution is twice as large as the total change in diametral strain anticipated based on the known maximum axial strain for these test conditions. However, the optical measurement system does give good data for tests conducted at higher strains as will be shown in a future report on the viscoplastic and damage results.

Second, the material was shown to have a moderate transverse texture (Fig. 3), and also displayed a directional dependence of the dynamic modulus (Fig. 4). Moreover, the material was not strictly transversely isotropic since there were slight differences in the degree of planar orientation between the transverse and thickness direction of the original rolled plate. The test samples were cylindrical with the load axis parallel to the rolled direction of the plate and the location of the other two plate directions were not maintained during machining. Hence the diametral extensometer measured the displacement of the diameter in some random and unknown transverse direction on the circumference of the samples.

Correctly treating the material as orthotropic would have resulted in three independent Poisson's ratios and would have required a great deal more testing to determine these values. Since the two transverse directions were not greatly different from one another, we considered treating the material as transversely isotropic, but still lacked sufficient data to determine all Poisson's ratios. The simplifying assumption of isotropy was believed to be somewhat justified since the texture is moderate in nature; therefore, to calculate Poisson's ratio ν we utilized

$$\nu = \frac{-e_t}{e} \tag{4}$$

Where e_t is transverse strain and e is axial strain.

In spite of the above-mentioned complications, we felt that there was still value in reporting selected data on transverse strains. Even though the signal-to-noise ratio is poor, trends can still be discerned in the data. Likewise, trends can also be observed in Poisson's ratio (assuming isotropy) even if the absolute values may be questionable. Finally, there are very few transverse stress-strain curves presented in the literature, and we thought that showing such curves would be of general interest.

An example of the transverse strain response measured is described via sample 25, tested at 427 °C. Its general behavior is typical of the tests at the other temperatures. The first test of this series is shown in Figure 39 for a creep test at a stress of 34 MPa and then in Figure 40 for its respective recovery at zero load. The axial strain response has already been shown in Figure 26. Figure 39 indicates that the total diametral strain initially increases (becomes more negative, or the diameter shrinks) during the loading and the first 30 000 s of creep, thereafter reaching an apparent constant average value of –258 με. The calculated isotropic value of Poisson's ratio for the loading portion of this test was 0.37. Upon unloading (Fig. 40) the diametral strain decreases (diameter expands) and reaches a constant value of –200 με almost immediately during the recovery phase. Although the transverse strain did not return to zero, it did shut down. Moreover, the axial strain at the end of recovery (Fig. 26) also failed to return precisely to zero. We suspect that both of these nonzero values fall within experimental scatter.

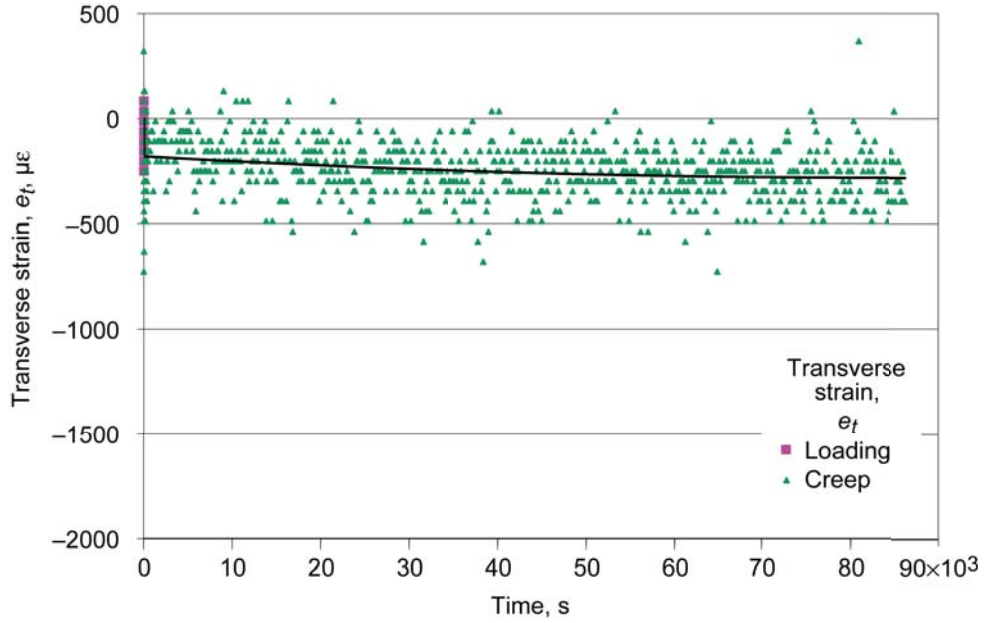

Figure 39.—Transverse strain during viscoelastic creep in reversible regime for Ti-6Al-4V at 427 °C.

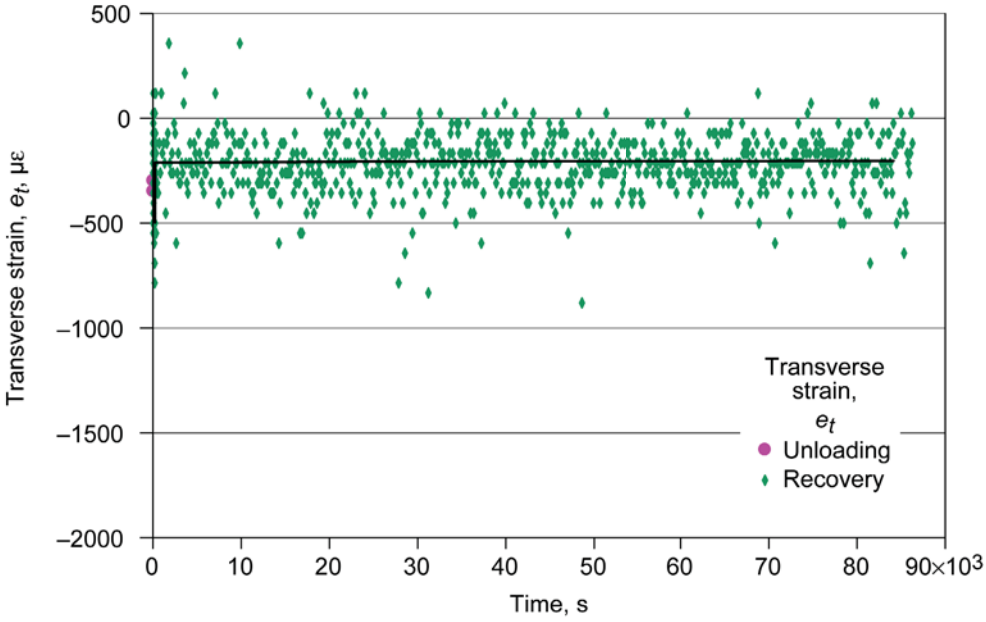

Figure 40.—Transverse strain during recovery in the reversible regime Ti-6Al-4V at 427 °C.

The next step in this test series was a relaxation test (25R) at an axial strain of 430 με. The corresponding axial strain and the stress response were shown in Figures 27 and 28. The diametral strains for the relaxation and recovery phases of this test are plotted in Figures 41 and 42, respectively. After a slight increase during the loading period, the diametral strain remains constant at a strain of –120 με during the relaxation period. During the recovery, no discernible decrease in transverse strain is observed after the specimen is unloaded. The diametral values remain constant at approximately –70 με. Again the diametral strain did not return completely to zero, but returned to a value less than half that observed in the previous test (25C). It should also be noted that unlike the previous load-controlled creep test, which showed primary

creep strains in both the axial and transverse directions, this strain-controlled relaxation test exhibited no change (as expected if Poisson's ratio is constant in time) from a constant value in either the axial or the transverse strain during the 24-h hold time.

The third test in this series was a creep test, above the threshold, at 206 MPa (see Fig. 29). The corresponding diametral strain during this creep test is shown in Figure 43. Consistent with the axial strain, the diametral strain exhibits a primary creep regime followed by a secondary creep regime, with no appearance of ever reaching a saturation point. During the recovery period (Fig. 44) the diametral strain decreases, showing again a primary region followed by saturation at a transverse strain of approximately –97 με. There is no indication that with continued time the diametral strain (or the axial strain) would return to zero, suggesting that the deformation was indeed irreversible and permanent.

As stated previously, the viscoelastic model put forward by Saleeb and Arnold (Ref. 1) assumes coincidence of moduli, which implies time independency of Poisson's ratio, although this assumption could not be definitively confirmed or refuted by the present test program given the experimental limitations stated. In nearly every test conducted in this study, diametral strain was measured using an optical micrometer. As observed in Figures 39 and 40, the amount of noise in the diametral signal was quite high. However, in most cases a trend in the diametral strain could still be observed, and thus a calculation of Poisson's ratio could still be made at various times. It was shown that during viscoelastic creep tests (Fig. 39), the transverse strain eventually shut down during creep and recovered slightly after unloading (Fig. 40). During stress relaxation, the transverse strain remained unchanged during the relaxation period (Fig. 41). This is expected since the axial strain is being held constant during the test. Concurrently, the diametral strain decreases during unloading and remains constant during recovery (Fig. 42). During recovery in the reversible regime the diametral strains appear to have shut down, although not always at zero. A small diametral strain value (-6×10^{-5}) often remained (Fig. 42), but this is believed to be within the acceptable range of scatter and given the experimental setup, assumed to be zero.

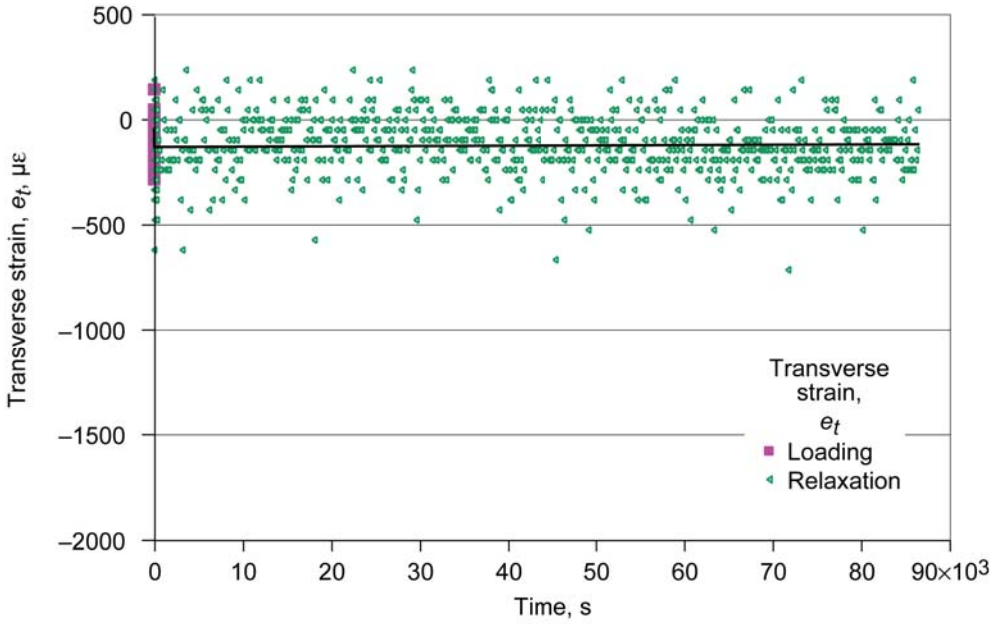

Figure 41.—Transverse strain during stress relaxation in the reversible regime Ti-6Al-4V at 427 °C.

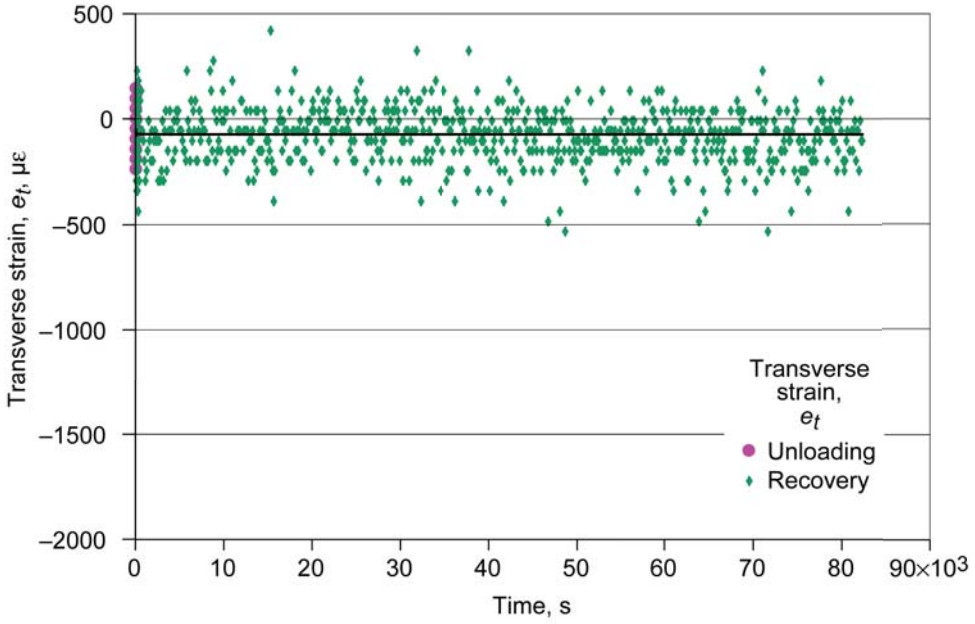

Figure 42.—Transverse strain during recovery in reversible regime for Ti-6Al-4V at 427 °C.

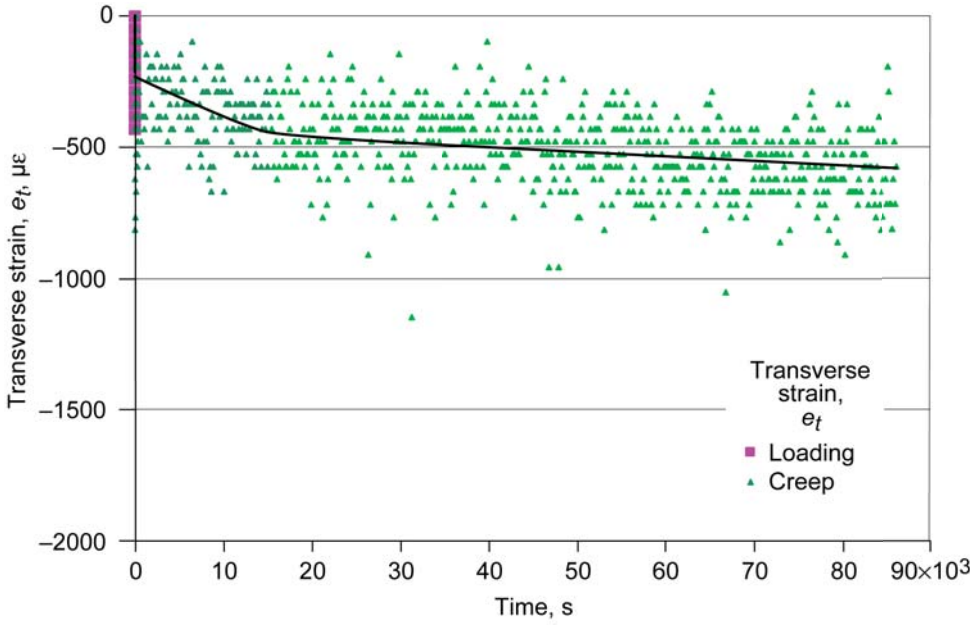

Figure 43.—Transverse strain during creep in irreversible regime for Ti-6Al-4V at 427 °C.

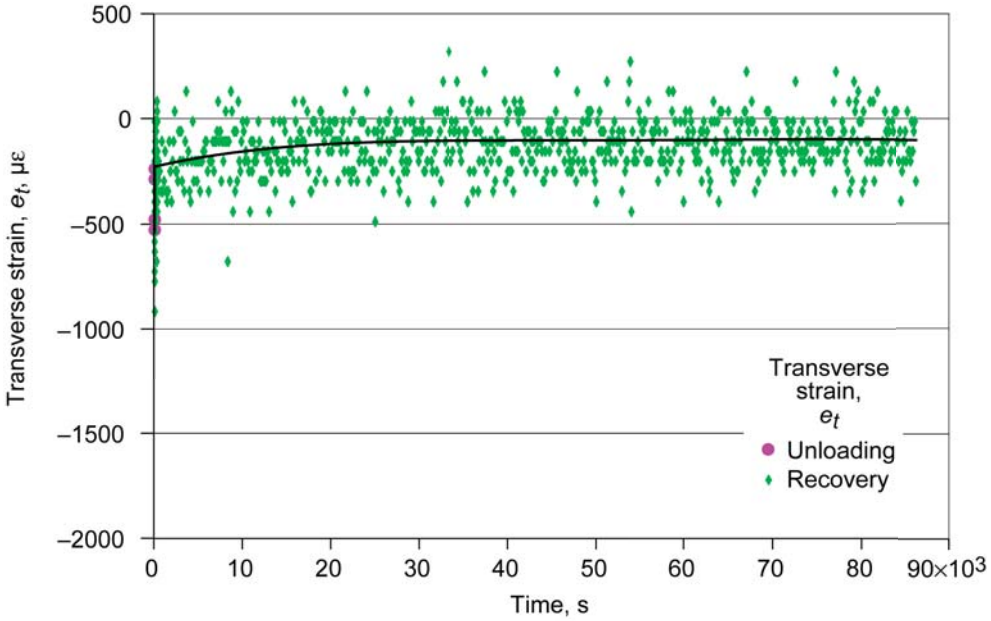

Figure 44.—Transverse strain during recovery in irreversible regime for Ti-6Al-4V at 427 °C.

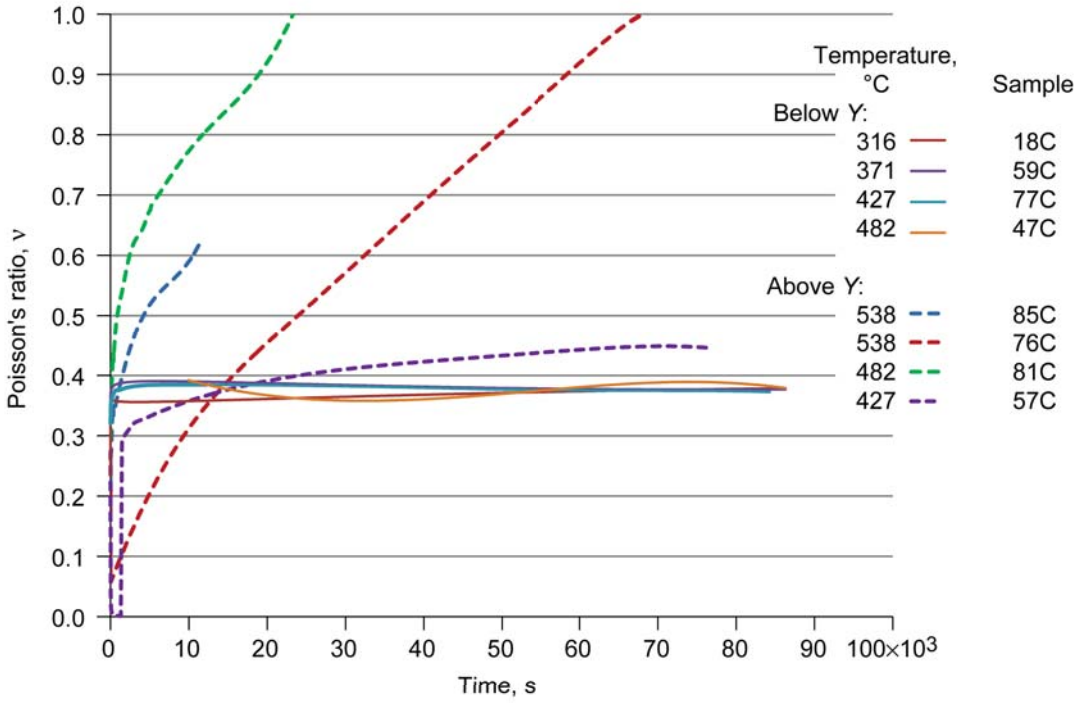

Figure 45.—Poisson's ratio for Ti-6Al-4V above and below axial threshold stress *Y* in both reversible and irreversible regimes at different temperatures.

A plot of Poisson's ratio over time for various creep samples tested at different temperatures is shown in Figure 45. There are two groups of data representing stress levels above and below the threshold *Y*. For those below the threshold, the calculated Poisson's ratio is approximately constant after the initial loading and yields an isotropic value of approximately 0.38. This is consistent with a range of values of 0.34 to 0.38 given by Fukuhara and Sanpei (Ref. 26) over the temperature range of 20 to 538 °C for Ti-6-4 using a dynamic method.

At stress levels above the threshold, Poisson's ratio continues to increase throughout the creep test. Three of the four tests exceed the isotropic plastic limit of 0.5. This could be due to two reasons: One, the material is orthotropic, permitting Poisson's ratio to reach higher values, and two, at least two of the samples entered tertiary creep and failed. Also localized necking was observed on these specimens, allowing more transverse strain to be measured than calculated through the Poisson's effect. Moreover, the orthotropic properties resulted in asymmetric necking forming an elliptical cross section at failure. Nonetheless, it is clear that the tests above the threshold had a significantly different Poisson's response than those beneath the threshold. Also, the behavior in the reversible regime appears to be constant and consistent with that idealized by the model.

A final note is made about the transverse measurements and the optical micrometer. The residual strain after recovery of a typical viscoelastic test is on the order of 60 με. This equates to a change in diameter of 0.4 μm. To show how small this value is and the difficulty in measuring it, the α-grain thickness for this material is 16 times larger. A speck of dust on the sample surface can be in the range of 4 to 50 μm, and the surface roughness of the machined sample could be as high as 1 μm. The possible errors introduced by any of these elements can be interpreted as transverse strains and could complicate the interpretation of the diametral strain values. Moreover, these errors are unique to the employed, noncontacting micrometer in which the micrometer is fixed on the load frame and the sample translates during loading within a fixed beam of light from the micrometer. Any variation in diameter along the gage length will be recorded as a change in the apparent diametral strain. At high temperatures surface oxidation can also increase the diameter and could be interpreted as a possible drift in transverse strain, although this aspect was thought to be insignificant in most of these tests. If future examination of Poisson's ratio is desired in the viscoelastic regime with the goal of documenting Poisson's ratio constancy throughout the creep tests, a specific and improved test setup would be required. A different sample geometry, such as a parallelepiped with a large specimen width to increase transverse strains, could be used. Otherwise a special high-resolution extensometer would need to be developed.

References

1. Saleeb, A.F.; and Arnold, S.M.: A General Time Dependent Constitutive Model: Part I—Theoretical Developments. J. Eng. Mater. Technol. Trans. ASME, vol. 123, 2001, pp. 51–64.
2. Arnold, S.M.; Saleeb, A.F.; and Castelli, M.G.: A General Time Dependent Constitutive Model: Part II—Application to a Titanium Alloy. J. Eng. Mater. Technol. Trans. ASME, vol. 123, 2001, pp. 65–73.
3. Saleeb, A.F., et al.: A General Hereditary Multimechanism-Based Deformation Model With Application to the Viscoelastoplastic Response of Titanium Alloys. Int. J. Plasticity, vol. 17, 2001, pp. 1305–1350.
4. Saleeb, A.F.; and Arnold, S.M.: Specific Hardening Function Definition and Characterization of a Multimechanism Generalized Potential-Based Viscoelastoplasticity Model. Int. J. Plasticity, vol. 20, 2004, pp. 2111–2142.
5. Donachie, M.J., Jr.: TITANIUM: A Technical Guide. ASM International, Metals Park, OH, 1988, p. 13.
6. AMS Specification 4911: Titanium Ti 6AL 4V. ASM Aerospace Specification Metals, Pompano Beach, FL.
7. ASTM E1876–09: Standard Test Method for Dynamic Young's Modulus, Shear Modulus, and Poisson's Ratio by Impulse Excitation of Vibration. ASTM International, West Conshohocken, PA, 2009.
8. ASTM E1012-12e1: Standard Practice for Verification of Test Frame and Specimen Alignment Under Tensile and Compressive Axial Force Application. ASTM International, West Conshohocken, PA, 2012.
9. Stephens, J.J.; and Munford, J.W.: Stress Relaxation of a Titanium (Ti-6Al-4V) Threaded Joint. Sandia Report Sand 87–1818, 1988, p. 5.

10. ATI Technical Data Sheet. ATI Ti-6Al-4V, Grade 5, Allegheny Technologies Incorporated, Pittsburgh, PA, 2012. http://www.atimetals.com/Documents/ati_6-4_tds_en_v1.pdf Accessed Apr. 17, 2014.
11. Aerospace Structural Metals Handbook. Vol. 4, 1997.
12. Chakrabarti, A.K.; and Nichols, E.S.: Creep Behavior of Cast Ti-6Al-4V Alloy. Titanium '80, Science and Technology; Proceedings of the Fourth International Conference on Titanium, Kyoto, Japan, vol. 2, 1980, pp. 1081–1096.
13. Wapniarsky, S.; Rotem, A.I.; and Rosen, A.: Creep of Ti-6Al-4V Titanium Alloy at Room Temperature. Strength of Metals and Alloys (ICSMA 9); Proceedings of the 9th International Conference, Technion—Israel Institute of Technology, Haifa, vol. 1, 1991, pp. 437–442.
14. Odegard, B.C.; and Thompson, A.W.: Low Temperature Creep of Ti-6Al-4V. Metall. Trans., vol. 5, 1974, pp. 1207–1213.
15. Katcher, M.: Creep of Titanium Alloys. Metal. Eng. Q., 1968, pp. 19–27.
16. Chiu, S.S.; Eftis, J.; and Jones, D.L.: Prediction of Fatigue Life With and Without Hold Times Using the Chaboche Viscoplastic Constitutive Theory. J. Eng. Mater. Technol. Trans. ASME, vol. 112, no. 2, 1990, pp. 188–197.
17. Imam, M.A.; and Gilmore, C.M.: Room Temperature Creep of Ti-6Al-4V. Metall. Trans., vol. 10A, 1979, pp. 419–425.
18. Evans, W.J.: Stress Relaxation and Notch Fatigue in Ti-6Al-4V. Scrip. Metal., vol. 21, 1987, pp. 1223–1227.
19. Hatch, A.J.; Partridge, J.M.; and Broadwell, R.G.: Room-Temperature Creep and Fatigue Properties of Titanium Alloys. J. Mater., vol. 2, no. 1, 1967, pp. 111–119.
20. Thompson, A.W.; and Odegard, B.C.: The Influence of Microstructure on Low Temperature Creep of Ti-5Al-2.5Sn. Metall. Trans., vol. 4, 1973, pp. 899–908.
21. Savage, M.F.; Neeraj, T.; and Mills, M.J.: Observations of Room-Temperature Creep Recovery in Titanium Alloys. Metall. Trans., vol. 33A, 2002, pp. 891–898.
22. Materials Properties Handbook: Titanium Alloys, R. Boyer, G. Welsch, and E.W. Collings, eds., ASM International, Materials Park, OH, 1994, p. 921.
23. Sinha, N.K.: Limitations of Stress Relaxation Tests for Determining Stress Dependence of Strain Rate at High Temperatures. Scripta Materialia, vol. 48, 2003, pp. 731–736.
24. Sinha, N.K.; and Kearsey, R.: Optimizing Deformation Path for Stress-Relaxation Tests on Superalloys at High Temperatures. ASME 2001–GT–421, 2001.
25. Sinha, N.K.: Short Strain Relaxation/Recovery Tests for Evaluating Creep Response of Nickel-Base Superalloys Like IN–738LC. J. Mater. Sci. Lett., vol. 20, 2001, pp. 951–953.
26. Fukuhara, M.; and Sanpei, A.: Elastic Moduli and Internal Frictions of Inconel 718 and Ti-6Al-4V as a Function of Temperature. J. Mat. Sci. Lett., vol. 12, 1993, pp. 1122–1124.